European Journal of Pharmacology 978 (2024) 176767

Contents lists available at ScienceDirect

European Journal of Pharmacology

journal homepage: www.elsevier.com/locate/ejphar

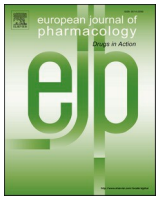

Fenofibrate reduces cardiac remodeling by mitochondrial dynamics preservation in a renovascular model of cardiac hypertrophy

Laura Castiglioni [a], Paolo Gelosa [a], Majeda Muluhie [a], Benedetta Mercuriali [a], Joanna Rzemieniec [a], Marco Gotti [a], Fabio Fiordaliso [b], Giuseppe Busca [c], Luigi Sironi [a,*]

[a] Department of Pharmaceutical Sciences, University of Milan, Milan, Italy
[b] Department of Molecular Biochemistry and Pharmacology, Istituto di Ricerche Farmacologiche Mario Negri IRCCS, Milan, Italy
[c] Azienda "Polo Veterinario di Lodi", University of Milan, Milan, Italy

ARTICLE INFO

Keywords:
Fenofibrate
Hypertension
Cardiac hypertrophy
Mitochondrial dynamics
Oxidative stress

ABSTRACT

Fenofibrate, a PPAR-α agonist clinically used to lower serum lipid levels, reduces cardiac remodeling and improves cardiac function. However, its mechanism of action is not completely elucidated. In this study we examined the effect of fenofibrate on mitochondria in a rat model of renovascular hypertension, focusing on mediators controlling mitochondrial dynamics and autophagy.

Rats with two-kidney one-clip (2K1C) hypertension were treated with fenofibrate 150 mg/kg/day (2K1C-FFB) or vehicle (2K1C-VEH) for 8 weeks. Systolic blood pressure and cardiac functional were *in-vivo* assessed, while cardiomyocyte size and protein expression of mediators of cardiac hypertrophy and mitochondrial dynamics were *ex-vivo* examined by histological and Western blot analyses.

Fenofibrate treatment counteracted the development of hypertension and the increase of left ventricular mass, relative wall thickness and cross-sectional area of cardiomyocytes. Furthermore, fenofibrate re-balanced the expression Mfn2, Drp1 and Parkin, regulators of fusion, fission, mitophagy respectively. Regarding autophagy, the LC3-II/LC3-I ratio was increased in 2K1C-VEH and 2K1C-FFB, whereas the autophagy was increased only in 2K1C-FFB.

In cultured H9C2 cardiomyoblasts, fenofibrate reversed the Ang II-induced mRNA up-regulation of hypertrophy markers Nppa and Myh7, accumulation of reactive oxygen species and depolarization of the mitochondrial membrane exerting protection mediated by up-regulation of the Uncoupling protein 2.

Our results indicate that fenofibrate acts directly on cardiomyocytes and counteracts the pressure overload-induced cardiac maladaptive remodeling. This study reveals a so far hidden mechanism involving mitochondrial dynamics in the beneficial effects of fenofibrate, support its repurposing for the treatment of cardiac hypertrophy and provide new potential targets for its pharmacological function.

1. Introduction

Hypertension is a major independent risk factor for cardiovascular morbidity and mortality (Egan, 2010; Frohlich, 1999) since it induces cardiac remodeling associated with left-ventricular hypertrophy leading to heart failure (Roger, 2013). Hypertension-induced cardiac hypertrophy is a complex pathological process, and involves multiple cellular events and molecular mechanisms, which are not well understood.

Currently, there are several pharmacological strategies that are effective for partial regression of cardiac hypertrophy by minimizing the neurohumoral activation involving renin-angiotensin system and sympathetic nervous system. According to the expert consensus, angiotensin-converting enzyme inhibitor (ACEI) and angiotensin receptor blockers (ARBs) are recommended as 1st-line therapeutic drugs (Chen et al., 2020). Angiotensin receptor-neprilysin inhibitors (Martens et al., 2018) and sodium–glucose cotransporter-2 (SGLT2) inhibitors (Brown et al., 2020) have been reported to be effective in reducing cardiac hypertrophy. Compared with other therapies, β-blockers are less effective in reversing hypertrophy, and several studies found no effect on reverse remodeling (Martin et al., 2023). Calcium channel blockers have only limited additional benefit (Fak et al., 1996), but improve their effectiveness when used as an add-on treatment with RAAS antagonists

* Corresponding author. University of Milan, Milan, Italy, Department of Pharmaceutical Sciences, via Balzaretti, 9, 20133, Milano, Italy.
E-mail address: luigi.sironi@unimi.it (L. Sironi).

https://doi.org/10.1016/j.ejphar.2024.176767
Received 6 March 2024; Received in revised form 20 June 2024; Accepted 20 June 2024
Available online 21 June 2024

or thiazide diuretics (Ahmed et al., 2020; Sun et al., 2011). Modest reverse remodeling has also been observed with cardiac myosin inhibitors and mTOR inhibitors (Paoletti et al., 2012; Saberi et al., 2021). Finally, PDE5 inhibitor sildenafil added to RAAS inhibition and β-blockade increases hypertrophy regression (Guazzi et al., 2011).

Despite existing pharmacological therapies ensure an improved health outcomes and regression of cardiac hypertrophy, a subset of patients are non-responding and full normalization of left ventricular mass in most patients does not occur even after years of treatment (Cuspidi et al., 2006). Many factors could have a role in determining whether and to what extent reverse remodeling occurs with existing therapies.

Among them, mitochondrial dysfunction has been indicated as a potential and important player in the development of cardiac hypertrophy (Torrealba et al., 2017). Growing evidence suggested that changes in "mitochondrial dynamics", which refers to processes of mitochondrial fusion, fission, biogenesis and mitophagy, may act as mechanisms for bioenergetic adaptation during cardiac pathological remodeling (Vásquez-Trincado et al., 2016). Unbalances of mitochondrial dynamic together with altered mitophagy were showed to play a functional role in the progression of cardiovascular diseases, such as myocardial infarction and hypertrophy (Hasan et al., 2018; Nah et al., 2017). Thus, mitochondrial dynamics is currently suggested as potential new therapeutic target, but its pharmacological modulation to improve cardiac remodeling requires further studies.

Of note, hypertrophic stimuli, including hypertension, induce down-regulation of peroxisome proliferator-activated receptor-α (PPARα) in cardiomyocytes and this is associated with a shift in energy substrate preference from fatty acid to glucose (Ismael et al., 2015), while targeting PPARα was suggested as potential option for the prevention of cardiac hypertrophy (Kar and Bandyopadhyay, 2018).

The agonists of PPAR-α receptor are currently used in clinical treatment of hypertriglyceridemia and type III hyperlipidaemia. In addition to lipid regulation, PPAR-α activation have shown anti-atherogenic potential by inhibition of vasculature inflammatory responses, as the cytokine-induced vascular cell adhesion molecule-1 (VCAM-1), thus limiting the recruitment of inflammatory cells to the activated endothelium (Marx et al., 1999). In addition, the vaso-protective effects of PPARα activation is achieved by enhancing endothelial nitric oxide (NO) synthase expression and NO release (Omura et al., 2001). Several animal studies of myocardial infarction reported beneficial effects of PPARα agonists by reducing infarct sizes and improving cardiac function (Wagner and Wagner, 2020), suggesting a role of PPAR-α agonists in the myocardial infarction. However, the absolute treatment effects of fibrates in the primary prevention of cardiovascular events appear to be modest and only in specific high-risk populations, in patients with type 2 diabetes mellitus and dyslipidemia (Keech et al., 2005; Rubins et al., 1999). In cardiac hypertrophy, PPARα could negatively regulate the cardiomyocyte hypertrophy by down-regulation of myocardial lipid and glucose metabolism (Zou et al., 2013), inhibition of PI3K/Akt/mTOR signaling pathways (Balakumar et al., 2019), regulation of nuclear HMGB1 expression (Jia et al., 2014a), reduction of ADAM17 (a disintegrin and metalloproteinase-17) expression (Zeng et al., 2018) and inactivation of adiponectin (Jen et al., 2017). However, other possible molecular mechanisms regulating the inhibition of cardiomyocyte hypertrophy by activated PPARα remain to be elucidated, in particular the prevention of mitochondrial impairment, as suggested (Castiglioni et al., 2018a; Kar and Bandyopadhyay, 2018). Relevantly, a study showed for the first time that cardiac-specific over-expression of PPARα induces a substantial restoration of mitochondrial structural integrity and function in models of cardiac hypertrophy (Rana et al., 2019).

The two-kidney one-clip (2K1C) rat model, developed by Goldblatt (Goldblatt et al., 1934), is commonly used as an experimental model for the study of renovascular hypertension. In this model, the partial occlusion of one renal artery induces an increased renin secretion and, consequently, hyper-activation of renin-angiotensin-aldosterone system (RAAS), persistent increase in blood pressure and cardiac hypertrophy (Martinez-Maldonado, 1991; Thöne-Reineke et al., 2003). In this animal model, the activation of PPARα by fenofibrate has been shown to attenuate hypertension (Sporková et al., 2017), while the increased expression of myocardial PPARα is one of the possible mechanisms by which apigenin improves cardiac hypertrophy (Zhu et al., 2016). However, to the best of our knowledge, no study has assessed the effects of fenofibrate on cardiac tissue in 2K1C hypertensive rats.

This study tested the possibility that treatment with fenofibrate blunts the development of 2K1C hypertension-associated left ventricular remodeling. In particular, we evaluated, in these hypertensive rats, the effect of fenofibrate on cardiac dysfunction, fibrotic processes, cardiomyocyte size and protein expression of endogenous mediators regulating cardiac hypertrophy In addition, we assessed the protein expression of key regulators of mitochondrial dynamics and mitophagy/autophagy, to identify possible novel mechanisms involved in the cardioprotection of fenofibrate and to provide the basis for potential targets in the treatment of cardiac hypertrophy.

2. Materials and methods

2.1. Experimental protocol

The procedures concerning animal care, surgery and euthanasia were carried out in accordance with Italian laws and with the current European Union Council (2010/63/UE) guidelines for the use of laboratory animals in chronic studies. The study was approved and authorized by the National Ministry of Health and University of Milan Committee (Approval number 778/2015-PR).

This study involved 7 weeks old male Wistar Kyoto rats (WKY, n = 36) (Charles River, Germany) (Fig. 1). Renovascular hypertension was induced with the 2-Kidney 1-Clip method (Zhu et al., 2009) (2K1C, n = 27) (T0). Briefly, rats weighing 180–200 g were anaesthetized by intraperitoneal injection of sodium pentobarbital (40 mg/kg). After a retroperitoneal flank incision, the left renal artery was separated from the renal vein by blunt dissection and then partly occluded by placing a U-shaped silver clip with an internal diameter of 0.20 mm. The normotensive sham-operated (n = 9) rats underwent the same procedure, without application of the silver clip. Operation time per animal did not exceed 15 min, during which the body temperature was continuously monitored and maintained at 37 ± 0.5 °C until awakening. Three 2K1C rats died within 1 week after surgery.

After four weeks (T1), blood was collected from tail vein and systolic arterial blood pressure (SBP) was measured, in order to confirm the onset of hypertensive condition (compared to sham-operated rats). In line with literature(da Silva et al., 2021; Gutsol et al., 2022; Smith and Bishop, 1986) and supported by our previous unpublished data, the 2K1C rats with SBP ≥140 mm Hg were included in the study. Nine 2K1C rats were instead excluded because SBP did not meet our inclusion criterion.

All the rats included into the study (2K1C, n = 15 and sham-operated, n = 9) underwent a cardiac magnetic resonance imaging (cMRI) analyses to determine cardiac parameters before starting treatment, and then the 2K1C rats (n = 15) were randomly assigned to each experimental group using the Microsoft excel RAND.BETWEEN function and treated orally by gavage for 8 weeks with vehicle (1% carboxymethyl cellulose) (2K1C-VEH, n = 8) or fenofibrate (FFB; Sigma-Aldrich, Germany) 150 mg/kg/day (2K1C-FFB, n = 7).

At the end of experimental protocol (T2, 12 weeks after surgical procedures, which also correspond to 8-week treatment), blood was collected from tail vein and SBP measurement and cMRI were performed. Then, rats were euthanized after administration of mixture of xylazine hydrochloride (10 mg/kg) and ketamine hydrochloride (90/mg/kg), and hearts were quickly removed and divided in two axial slices of about 2-mm-thickness at mild papillary level. One slice was frozen at −80 °C for Western blot analysis, while the other one was fixed in 10%

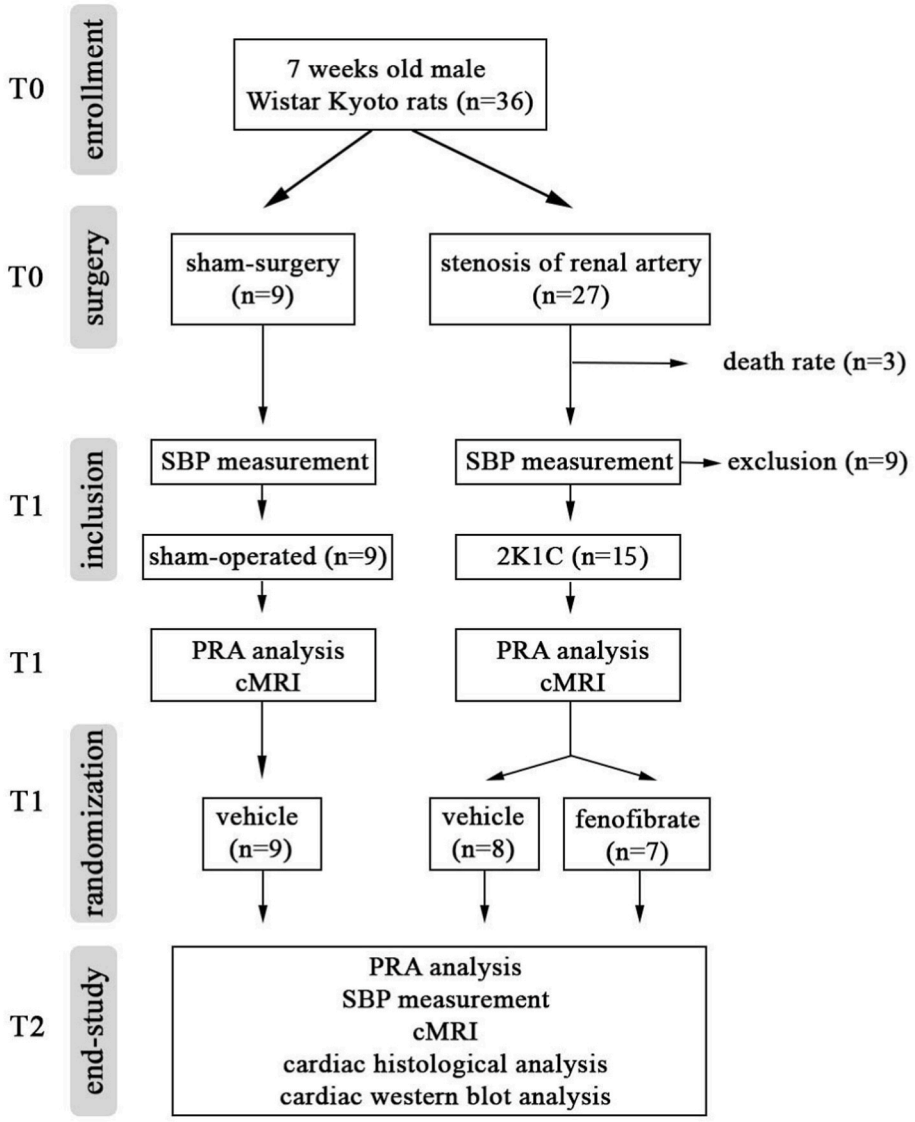

Fig. 1. Study protocol. After a period of acclimatization, thirty-six WKYs were assigned to two experimental groups (day 0). Twenty-seven (2K1C) rats were subjected to a two-kidney, one-clip (2K1C) model, whereas nine rats were sham-operated.
At week 4 (T1), blood was collected and systolic arterial blood pressure (SBP) and cardiac MRI analysis were performed. Fifteen 2K1C untreated rats with systolic blood pressure (SBP) > 140 mm Hg were included in the study, randomized into 2 subgroups treated orally by gavage for 8 weeks with vehicle (1% carboxymethyl cellulose) (2K1C-VEH, n = 8) or fenofibrate (150 mg/kg/day, 2K1C-FFB, n = 7). At the end of the experiment (week 12, T2), rats were subject to cMRI and SBP measurements, and blood and hearts were collected for ex-vivo analysis.

formalin (Merck, Germany) overnight at 4 °C for histological analysis.

2.2. Systolic blood pressure measurement

Systolic arterial blood pressure was measured in rats by means of tail-cuff plethysmography (BP-2000, Visitech Systems, USA). In detail, conscious rats were restrained on a heated plate at 37 °C. Cuffs were set up at the base of the tails and connected to a data acquisition system. The rats from all experimental groups were trained to the restraint at least three times in one week before the baseline measurements. At least three consecutive pressure determinations were made for each animal and the average of these was recorded as the SBP for that animal.

2.3. Cardiac magnetic resonance imaging (MRI) experiments

Cardiac magnetic resonance imaging was performed using a 4.7T vertical-bore MR magnet (Bruker spectrometer AMX3 with micro-imaging accessory, Germany). Anesthesia was induced by exposing rats to 3% isoflurane (Merial, France) in 0.4 ml/min of O_2 and 2.0 ml/min of N_2 in an induction chamber. Rats were then fixed on a holder, anaesthetized with inhaled 1% isoflurane, and placed into the vertical, 15-cm bore spectrometer equipped with a 6.4 cm diameter birdcage coil. During the acquisitions, the respiration was monitored.

A series of scout images were first acquired to define landmark points for the acquisition of the long-axis 4 chamber view and then, orthogonally to it, the short-axis sections (Franzosi et al., 2011).

The images were acquired using a retrospective gated cine gradient echo sequence with the following parameters: echo time (TE) 1.91 ms; repetition time (TR) 10.75 ms, field of view 4 × 4 cm^2; acquisition matrix 128 × 128 pixels; slice thickness 2 mm; 6–8 axial slices spaced 1.8 mm to fully cover the left ventricle (LV). The MR data were acquired in multiple contiguous short-axis slices, using 12 frames for every cardiac cycle.

Then, the images were analyzed using custom software implemented in Python, along the lines of Franzosi et al. (2011) in order to obtain LV parameters as end-diastolic (LV EDV), end-systolic (LV ESV) and stroke

volumes (LV SV), ejection fraction (LV EF), mean internal systolic and diastolic diameters, mean diastolic and systolic wall thicknesses (LV ThWd and LV ThWs) and derived MRI relative wall thickness (RWT) and LV mass.

Briefly for each frame the short-axis images were cropped manually selecting a region of interest (ROI) surrounding the LV on the end-diastolic frame. In each images the endocardial border was manually detect, then the area of the LV cavity was computed. For each short-axis slice an Area max and Area min were detected as the frames with maximum and minimum number of pixel, respectively. End diastolic and end systolic volumes (LV EDV and LV ESV) were then computed as sum of Area max and Area min for each short-axis slice multiplied by the slice thickness. Stroke volume (LV SV) and ejection fraction (LV EF) were derived.

On mid papillary diastolic and systolic frames, epicardial borders were manually traced and 18 concentric rays were obtained starting from a point manually placed at the junction between the right ventricular free wall and the interventricular septum. Systolic and diastolic internal diameters were computed as 2 * mean distance between endocardial border and centroid; diastolic and systolic wall thickness (LV ThWd and LV ThWs) as mean distance between the endocardial and epicardial borders along the eighteen consecutive rays. Relative wall thickness and LV mass were computed.

2.4. Plasma renin activity determination

Plasma renin activity (PRA) was determined by incubating plasma samples at 37 °C for 1 h, and using a commercial radioimmunoassay kit to measure the generated angiotensin I, which was expressed as ng/ml per h. As plasma renin concentrations are extremely low, a sensitive and reproducible plasma renin test can only be made by means of the PRA radioimmunoassay (Sealey et al., 2005).

2.5. Western blot analysis for protein expression

Myocardial LV samples were pulverized in liquid nitrogen, and then a portion (60–90 mg) was homogenized by dispenser (T 25 ULTRA-TURRAX – IKA, Germany) on ice in 10 vol of RIPA lysis buffer (150 mM NaCl, 10 mM, Tris, pH 7.4, 5 mM EDTA, 0.1% SDS, 1% sodium deoxycholate and 1% Triton X-100) added with protease inhibitors (Roche Diagnostics, Germany) and phosphatase inhibitors (Sigma-Aldrich, Germany) according to manufacturer's instructions. The homogenates were spin (13.000 rpm for 15 min at 4 °C) and the supernatants were collected and assayed for protein quantification by Bradford method (Bradford, 1976). Aliquots of the protein extracts were separated into single-use samples and stored at −80 °C until use.

An aliquot of 70–90 μg of protein from each sample was separated on 8–15% SDS-polyacrylamide gel by electrophoresis and then transferred to nitrocellulose membranes using iBlot 2 Dry Blotting System (Thermo Fisher Scientific, USA). The membranes were reversibly stained with Ponceau S and then blocked with 5% non-fat dry milk in TBS-TWEEN 20 0.1% at room temperature for 1 h. Subsequently, the membranes were incubated with specific primary antibodies (Table 1) overnight at 4 °C with gentle shaking. Next, the membranes were washed and incubated with goat anti mouse HRP-labeled secondary antibody (Bio-Rad Laboratories, USA) (1:2500 in 5% non-fat dry milk in TBS-TWEEN 20 0.1%) or with goat anti rabbit HRP-labeled secondary antibody (Sigma Aldrich, Germany) (1:2500 in 5% non-fat dry milk in TBS-TWEEN 20 0.1%) at room temperature for 2 h.

Membranes are horizontally cut to probe proteins with different molecular weights. Images of the original membranes were provided as supplementary data. When a single blot was analyzed sequentially with multiple antibodies, the first primary and secondary antibodies were removed by using stripping buffer (100 mM 2-mercaptoethanol, 2% (w/v) SDS, 62.5 mM Tris-HCl, pH 6.7.) for 45 min at 50 °C, and subsequently incubated with additional primary and secondary antibodies. The blots were visualized using ECL solution (Cyanagen, Italy).

Finally, the reaction products were densitometrically quantified using an Odyssey imaging system (LI-COR Biosciences, USA) and Image J software. The ratio of the protein of interest was subjected to GAPDH, which acted as the internal control in the experiments.

2.6. Histological analysis

Axial sections of 4-μm-thickness were prepared from paraffin-embedded cardiac tissue fixed in 10% formalin (Merck, Germany) and mounted on glass slides.

After de-paraffinization and re-hydration, cardiac sections were stained with standard hematoxylin-eosin and Sirius red F3BA (0.5% in saturated aqueous picric acid) (Gelosa et al., 2011) to evaluate media: lumen ratio of cardiac vessels and perivascular fibrosis, measured as ratio of the media area to the lumen area and as ratio of the fibrosis area surrounding the vessel to lumen area, respectively.

About 20 fields (648 μm × 864 μm), acquired using Axioskop (Zeiss, Jena, Germany) and Canon digital camera (Eos 40D, Japan), were randomly selected from three sections for each rat and recorded. Only vessels that appeared circular on cross section and with lumen diameter less than 100 μm were analyzed.

To assess cardiomyocyte cross sectional area, three sections for each rat were incubated overnight at 4 °C with wheat germ agglutinin (WGA)

Table 1
List of primary antibodies used for Western blot analysis.

Antigen	Host	dilution	polyacrylamide gel	Company	catalogue number
Akt	mouse	1:1000	10%	Cell Signaling (MA, USA)	2920
p-Akt	rabbit	1:500	10%	Cell Signaling (MA, USA)	4060
GSK3-α/β	rabbit	1:1000	10%	Cell Signaling (MA, USA)	5676
p-GSK3-β	mouse	1:500	10%	Cell Signaling (MA, USA)	14630
ERK1/2	rabbit	1:1000	10%	Cell Signaling (MA, USA)	9102
p-ERK1/2	mouse	1:500	10%	Cell Signaling (MA, USA)	9106
AMPK	mouse	1:1000	10%	Cell Signaling (MA, USA)	2793
p-AMPK	rabbit	1:500	10%	Cell Signaling (MA, USA)	2535
Drp1	rabbit	1:500	8%	Novus biologicals (CO, USA)	NB110-55237
Mfn2	rabbit	1:1000	9%	Cell Signaling (MA, USA)	9482
Parkin	rabbit	1:500	10%	Cell Signaling (MA, USA)	2132
beclin-1	rabbit	1:1000	10%	Cell Signaling (MA, USA)	3738
LC3A/B	rabbit	1:1000	15%	Cell Signaling (MA, USA)	4108
p62	rabbit	1:1000	10%	Sigma-Aldrich (MO, USA)	P0067
UCP2	rabbit	1:500	10%	Proteintech (IL, USA)	11081-1-AP
mTOR	mouse	1:1000	6.5%	Cell Signaling (MA, USA)	4517
p-mTOR	rabbit	1:500	6.5%	Cell Signaling (MA, USA)	5536
GAPDH	rabbit	1:500	10%	Santa Cruz (CA, USA)	sc-25778

conjugated to Alexa Fluor 488 (1:100; Invitrogen Carlsbad, CA, USA). Sections were then rinsed with PBS and nuclei were counterstained with Hoechst 33258. Immunofluorescence images (324 μm × 432 μm) were acquired at fixed exposure times using Axiovert 200M (Zeiss, Jena, Germany). Lines were drawn to delineate the border of each cell according to WGA staining that highlights the cell membrane, then the area within the border of transversally sectioned cardiomyocytes with circularity greater than 0.6 and round nuclei, were automatically calculated (Castiglioni et al., 2018a). Mean area was evaluated by measuring 150–200 cells per heart.

All quantitative analyses were performed using ImageJ, an open source software, by an investigator blinded to the experimental groups (n = 4 animals/group).

2.7. Culture of cardiomyocytes

In order to better elucidate the direct effect of fenofibrate treatment on cardiomyocyte, *in vitro* experiments were performed on H9C2 cell line, reported to be energetically similar to primary cardiomyocytes (Kuznetsov et al., 2015). The embryonic rat cardiomyocyte cell line H9C2 (H9c2(2-1) (ATCC® CRL-1446™)) were grown in culture medium (DMEM, Dulbecco's Modified Eagle Medium, 4.5 g/l D-glucose, 4 mM l-glutamine, 25 mM Hepes, plus penicillin 100U/ml and streptomycin 100 μg/ml) supplemented with 10% of fetal bovine serum (FBS) in a humidified incubator with 5% CO_2 at 37 °C. Cells between passages 45–48 were used. For all the experiments, when the cells reached 70% of confluence, the medium was substituted with DMEM (4.5 g/l D-glucose, 4 mM l-glutamine, 25 mM Hepes, 1% of penicillin/streptomycin) without FBS, to put the cells under starvation condition for overnight period. Then, cardiomyocytes were stimulated with Ang II (1 μM) (Sigma Aldrich, Germany) and treated with fenofibrate (0.1 μM) for 24 h. In detail, for 24 well plates, 7.5 μl of Ang II (100 μM in sterile water) and/or 0.75 μl of fenofibrate (100 μM in DMSO/PBS 0.01M (50/50, v/v)) were added to 750 μl of culture medium, whereas for 6 well plates 30 μl of Ang II (100 μM in sterile water) and/or 3 μl of fenofibrate (100 μM in DMSO/PBS 0.01M (50/50, v/v)) were added to 3 ml of culture medium without FBS.

For control condition the same volume of vehicles was added. For each analysis three independent experiments were performed.

2.8. Lactate dehydrogenase (LDH) leakage

Cytotoxicity was evaluated by detecting plasma membrane damage using commercially available LDH-estimation (Cytotoxicity detection Kit, Roche Diagnostic, GmbH, Mannheim, Germany). According to the manufacturer's instructions, cell-free culture supernatants were mixed with lactate dehydrogenase (LDH) reaction mixture and incubated for 30 min at room temperature. The absorbance was measured at 490 nm.

2.9. Measurement of cell surface area and UCP2 expression

H9C2 cardiomyocytes grown on 13 mm cover slides in 24 well plates were fixed with 4% paraformaldehyde for 10 min. Cells were permeabilized with Goat Serum Dilution Buffer (GSDB: 450 mM NaCl, 20 mM sodium phosphate buffer, pH 7.4, 15% goat serum, 0.3% Triton X-100) for 15 min. For measurement of cardiomyocytes surface area, labelling was performed incubating cells for 1 h at room temperature with Phalloidin-iFluor 488 (1:500 in GSDB, Abcam, Cambridge, United Kingdom). For UCP2, the staining for phalloidin was performed in colocalization with rabbit anti UCP2 (1:40 in GSBD, Proteintech, Manchester, UK). Secondary antibody goat anti rabbit biotin labeled (1:500 in GSDB, PerkinElmer, Monza, Italy) was applied for 2 h at room temperature.The signal intensity was enhanced using the High Sensitivity Tyramide Signal Amplification kit (PerkinElmer, Monza, Italy) following the manufacturer's instructions.

Nuclei were labeled using Hoechst 33258 (1:20,000, Life Technologies, Carlsbad, CA, USA). Cover slides were finally mounted with a fluorescent mounting medium (Dako, Glostrup, Denmark) and analyzed under a fluorescence microscope.

Fluorescence was analyzed using a confocal microscope A1R; Nikon, Tokyo, Japan). At least five randomly selected areas (883.88 μm × 883.88 μm for CSA, and 319.5 μm × 319.5 μm for UCP2) were chosen per cover slip (n = 3 per each group), and 10–20 cells were randomly selected in each area. Cell surface areas and positive area for UCP2 were measured using ImageJ software. Data were expressed as % of UCP2 positive area/cell surface area.

2.10. Measurement of ROS production

The presence of intracellular ROS was detected using dihydroethidium (DHE, Sigma Aldrich, Germany), a sensitive fluorescent dye. According to the manufacturer's instructions, sub-confluent cells grown on cover slides were incubated with 10 μM DHE at 37 °C for 30 min. Cover slides were mounted with a fluorescent mounting medium (Dako, Glostrup, Denmark) and fluorescence was captured with a confocal microscope A1R; Nikon, Tokyo, Japan). At least five randomly selected areas (880.65 μm × 880.65 μm) were chosen per cover slip (n = 3 per each group). DHE positive area were measured using ImageJ software. Data were expressed as % of DHE positive area/nuclear surface area.

2.11. Mitochondrial membrane potential assay

The mitochondria-specific cationic dye JC-1 (5, 5′, 6, 6′-tetrachloro-1, 1′, 3, 3′-tetraethylbenzi-midazol-carbocyanine iodide; Invitrogen Carlsbad, CA, USA) was used to detect mitochondrial membrane potential. As previously described (Castiglioni et al., 2018a), cells grown on 13 mm cover slides in 24 well plates were incubated with medium containing freshly prepared 5 μg/mL of JC-1 dye for 30 min at 37 °C.

The fluorescent signal was captured using a confocal microscopy (A1R; Nikon, Tokyo, Japan). The fluorescence red (emission at 590 nm) indicates membrane potential-dependent JC-1 aggregates in normal mitochondria. Green fluorescence (emission at 527 nm) reflects the monomeric form of JC-1 appearing in the cytoplasm after mitochondrial membrane depolarization in damaged mitochondria. Mitochondrial depolarization is indicated by a decrease in the red/green fluorescence intensity ratio. Red and green ratios were obtained using the pixel intensity tool within ImageJ software(Castiglioni et al., 2018a). At least five randomly selected areas (880.65 μm × 880.65 μm) were chosen per cover slide (n = 3 per each group).

2.12. RNA Isolation and quantitative RT-PCR

Total RNA from cells grown in 6 well plates was extracted with Direct-zol RNA microprep (Zymo-Research, Irvine, CA) according to manufacturer's instructions. RNA samples were quantified with a GE Healthcare NanoVue Plus UV–Vis Spectrophotometer and 1 μg of RNA was reversely transcribed into cDNA by using SensiFAST™ cDNA Synthesis Kit (Meridian Bioscience Cincinnati, Ohio). A quantitative PCR was carried out by SsoAdvancedTM Universal SYBR Green Supermix (Bio-Rad) using Bio-Rad CFX Connect real-time System (Bio-Rad). Each experiment was run in triplicate and changes in mRNA levels were expressed as 2-ΔΔCt values and presented relative to the mean of the RPL13a reference gene. Sequences of the PCR primers are shown in Table 1, and PCR conditions were set as follows: initial denaturation at 95 °C for 3 min, followed by 39 cycles at 95 °C for 10 s and 60 °C for 30 s.

2.13. Statistical analysis

Statistical analyses were performed using R (http://www.R-project.org). For all analyses at T1, before drug administration, an Helmert "a priori" orthogonal contrast was used to compare sham-operated group vs 2K1C untreated group in order to assess the effect of 4 weeks of renal

clip, and 2K1C-VEH *vs* 2K1C-FFB to check for correct group randomization. At T2, a Bartlett test was conducted to assess homogeneity of variances. One-way ANOVA parametric tests followed by a Tukey "post hoc" analysis or Kruskal-Wallis non-parametric tests followed by Dunn's "post hoc" analyses were used accordingly. For *in vitro* studies, One-way ANOVA parametric tests followed by Sidak multiple comparison "post-hoc" analysis were used.

The data were expressed as mean ± SEM. Differences with $P < 0.05$ were considered statistically significant.

3. Results

3.1. Fenofibrate improves hypertension and cardiac remodeling

After 4 weeks from renal stenosis, 2K1C rats showed a significant increase in SBP compared to sham-operated rats ($P < 0.001$; Table 2). After that, 8 weeks of fenofibrate treatment counteracted the further increase of SBP occurring in 2K1C-VEH ($P < 0.001$ *vs* sham-operated and $P < 0.01$ *vs* 2K1C-FFB). Instead, plasma renin activity (PRA) was not different among groups at 4 weeks (Table 2), but it dramatically increased in 2K1C-VEH rats, reaching 14.3 ± 3.0 ng/ml/h at 12 weeks from renal stenosis ($P < 0.05$ vs sham-operated). Treatment with fenofibrate partially prevented this increase (11.4 ± 1.7 ng/ml/h; $P = 0.53$).

Then, we characterized the pressure overload-induced cardiac remodeling under the present experimental settings by cMRI analysis (Table 3 and Fig. 2). We found that at 4 weeks after renal stenosis, there was a slight increase of LV diastolic wall thickness ($P = 0.36$) and relative wall thickness (RWT) ($P = 0.23$) in 2K1C rats. However, at 12 weeks, 2K1C-VEH rats developed a significant increase in LV mass ($P < 0.01$) and wall thickness ($P < 0.05$ for both end-diastolic and end-systolic) compared to sham-operated rats. Fenofibrate was able to decrease LV mass ($P < 0.01$), wall thickening ($P < 0.05$ and $P < 0.01$ for end-diastolic and for end-systolic, respectively) and RWT ($P < 0.05$) compared to 2K1C-VEH rats. Along the experiment, no differences were observed in LV end-diastolic volume (EDV), LV end-systolic volume (ESV), stroke volume (SV) and ejection fraction (EF) among groups.

The protective effect of fenofibrate on cardiac remodeling is also confirmed by the results of the cardiac histology (Fig. 3). In the heart of 2K1C-VEH rats, perivascular fibrosis was markedly increased versus sham-operated rats ($P < 0.05$), which was partially decreased in fenofibrate-treated rats ($P = 0.069$ *vs* 2K1C-VEH rats) (Fig. 3A). Fenofibrate was instead able to counteract the enhancement of medial wall thickness of cardiac arteries ($P < 0.05$) (Fig. 3B). Next, wheat germ agglutinin staining showed that fenofibrate treatment significantly ($P < 0.01$) prevented the increased cross-sectional area of cardiomyocytes which was observed in 2K1C-VEH rats ($P < 0.05$ *vs* sham-operated) (Fig. 3C).

To examine whether fenofibrate directly protects cardiomyocytes against stress-induced hypertrophy independently from hypertension, we used cultured H9C2 rat cardiomyocytes stimulated with Ang II for 24 h. Fenofibrate significantly diminished the Ang II-induced increase in cardiomyocyte size (Fig. 3D) and the mRNA expression of the hypertrophy marker genes Nppa (encoding the atrial natriuretic peptide, ANP) and Myh7 (encoding β-myosin heavy chain, β-MHC) (Fig. 3E). In our experimental condition Ang II treatment did not affect cytotoxicity (Fig. 3F).

Thus, these data provide strong evidence that fenofibrate exerts several beneficial ameliorative effects on hypertension-induced cardiac hypertrophy, improving both functional properties and tissue features of heart. These effects could be partially ascribed to a direct effect of fenofibrate on cardiomyocytes.

Table 2
Physiological parameters.

	Rats	Body Weight (g)	PRA (ng/ml/h)	SBP (mm Hg)
T1 = 4w surgery				
Sham-operated	9	323 ± 11	4.3 ± 0.3 (n = 4)	122 ± 4
2K1C untreated	15	311 ± 10	5.2 ± 0.8 (n = 8)	146 ± 2***
2K1C-VEH	8	305 ± 15	5.0 ± 1.1 (n = 4)	147 ± 3
2K1C-FFB	7	317 ± 14	5.4 ± 1.4 (n = 4)	146 ± 2
T2 = 12w surgery and 8w FFB treatment				
Sham-operated	9	374 ± 16	4.7 ± 0.8 (n = 4)	123 ± 3
2K1C-VEH	8	381 ± 15	14.3 ± 3.0 (n = 4) *	179 ± 13***##
2K1C-FFB	7	373 ± 14	11.4 ± 1.7 (n = 4)	141 ± 2

Values are presented as mean ± SEM. At T1 Helmert "a priori" orthogonal contrast was performed to compare sham-operated group vs 2K1C untreated group and to compare 2K1C-VEH vs 2K1C-FFB checking for unbiased randomization.
At T2 parametric one-way ANOVA followed by a Dunnet "post hoc" analysis or non-parametric Kruskal-Wallis followed by Holm - Bonferroni "post hoc" analyses were used. For Dunnet test 2K1C-VEH group used as comparator. *p < 0.05, ***p < 0.001 vs Sham-operated and ##p < 0.01 vs 2K1C-FFB.

3.2. Fenofibrate modulates signal-transduction hypertrophic pathways

Given the critical role of the mitogen-activated protein kinase (MAPK) pathway, Akt and glycogen synthase kinase (GSK-3) in the process of cardiac hypertrophy (Schirone et al., 2017), we evaluated the expression level and activity of ERK1/2, Akt and GSK3-β in our experimental model (Fig. 4A). The phosphorylated Akt was dramatically up-regulated in 2K1C-VEH rats when compared with sham-operated rats ($P < 0.05$), while fenofibrate treatment partially decreased the phosphorylation of Akt ($P = 0.10$) No changes were observed in phosphorylation of GSK3-β and ERK1/2 and in the total protein expression of Akt, ERK1/2, and GSK3-β among the groups.

In the last years, some studies have demonstrated the involvement of AMPK/mTOR signaling pathway in the regulation of cardiac growth in response to pressure overload (Sciarretta et al., 2014; Zhou et al., 2015). We found that the phosphorylation level of AMPK was not affected in 2K1C-VEH rats ($P = 0.95$), but it was significantly increased by fenofibrate treatment ($P < 0.001$ vs 2K1C-VEH; Fig. 4B). 2K1C-VEH rats showed instead a significant increase in phosphorylation of mTOR compared to sham-operated rats ($P < 0.01$; Fig. 4B), which was slightly counteracted by fenofibrate ($P = 0.22$).

Taken together, these results indicated that fenofibrate treatment suppressed cardiac hypertrophy inducing AMPK activation and, at least in part, attenuating Akt and mTOR.

3.3. Fenofibrate attenuates oxidative stress and instability of the mitochondria membrane potential, and modulates mitochondrial quality control signaling

To shed light on possible mechanisms of cardioprotective effects of fenofibrate, we firstly investigated the ROS production *in vitro*. As evidenced by DHE staining, Ang II markedly increased the fluorescence intensity in H92C cells ($P < 0.05$; Fig. 5A), indicating an increase of ROS production, which was significantly attenuated by fenofibrate treatment ($P < 0.05$; Fig. 5A).

As ROS are primarily generated in mitochondria, and mitochondrial abnormalities induce ROS overproduction, we secondly focused on mitochondria. Uncoupling protein 2 (UCP2) belongs to the family of mitochondrial anion carrier proteins whose effectiveness in reducing mitochondrial oxidative stress and modulation of mitochondrial function is well established (Tian et al., 2018). Its modulation is reported in models of pulmonary hypertension (Haslip et al., 2015), cardiac hypertrophy, ischemia, and aging (Akhmedov et al., 2015).

Our results showed that UCP2 protein expression was significantly decreased in H9C2 cells treated with Ang II ($P < 0.001$; Fig. 5B) and that fenofibrate was able to completely restore the UCP2 expression ($p < 0.01$; Fig. 5B). Moreover, the protein level of UCP2 was significantly decreased in 2K1C-VEH rats compared to sham-operated rats ($P < 0.05$).

Table 3
Left ventricular parameters.

	Rats	LV EDV (μl)	LV ESV (μl)	LV SV (μl)	LV EF (%)	LV ThWd (mm)	LV ThWs (mm)	LV mass (mg)	RWT
T1 = 4w surgery									
Sham-operated	9	356 ± 12	85 ± 8	271 ± 9	76 ± 2	1.59 ± 0.06	2.98 ± 0.07	555 ± 12	0.46 ± 0.02
2K1C untreated	15	317 ± 15	82 ± 7	235 ± 12	74 ± 2	1.72 ± 0.06	3.02 ± 0.07	572 ± 17	0.53 ± 0.03
2K1C-VEH	8	318 ± 14	78 ± 8	240 ± 12	76 ± 2	1.74 ± 0.07	3.11 ± 0.09	593 ± 26	0.52 ± 0.02
2K1C-FFB	7	316 ± 30	86 ± 11	230 ± 22	73 ± 2	1.70 ± 0.10	2.91 ± 0.11	547 ± 18	0.53 ± 0.06
T2 = 12w surgery and 8w FFB treatment									
Sham-operated	9	340 ± 17	88 ± 7	252 ± 12	74 ± 1	1.78 ± 0.03	3.06 ± 0.08	622 ± 16	0.53 ± 0.02
2K1C-VEH	8	369 ± 35	94 ± 14	274 ± 22	75 ± 1	2.15 ± 0.14* $^{\#}$	3.63 ± 0.16* $^{\#\#}$	789 ± 47** $^{\#\#}$	0.64 ± 0.06$^{\#}$
2K1C-FFB	7	412 ± 22	104 ± 11	307 ± 14	75 ± 2	1.71 ± 0.09	2.93 ± 0.16	592 ± 26	0.47 ± 0.04

Values are presented as mean ± SEM. At T1 Helmert "a priori" orthogonal contrast was performed to compare sham-operated group vs 2K1C untreated group and to compare 2K1C-VEH vs 2K1C-FFB checking for unbiased randomization.
At T2 parametric one-way ANOVA followed by a Dunnet "post hoc" analysis or non-parametric Kruskal-Wallis followed by Holm - Bonferroni "post hoc" analyses were used. For Dunnet test 2K1C-VEH group used as comparator. *$p < 0.05$, **$p < 0.01$ vs sham-operated and $^{\#}p < 0.05$, $^{\#\#}p < 0.01$, $^{\#\#\#}p < 0.001$ vs 2K1C-FFB.

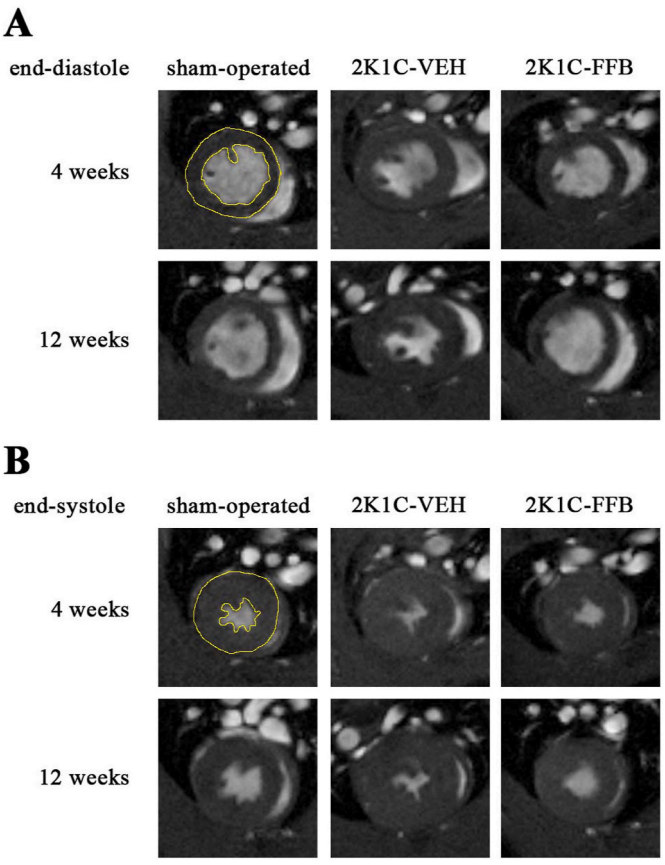

Fig. 2. Fenofibrate improves left ventricular cardiac hypertrophy. Representative axial cardiac MRI images of the end-diastolic **(A)** and of the end-systolic **(B)** mid papillary frames, taken from sham-operated, 2K1C-VEH or 2K1C-FFB rats. Images were taken from the same animals at T1 (week 4) and T2 (week 12). In the images of the sham-operated rat, the dashed lines delimit the left ventricle.

This effect was partially counteracted by fenofibrate, which increased UCP2 protein by 50% ($P = 0.63$) (Fig. 5B).

JC-1 staining revealed that Ang II stimulation led to a decrease in the red/green fluorescence ratio ($P < 0.05$; Fig. 5C), indicating a depression of mitochondrial membrane potential ($\Delta\Psi m$) which was reversed by fenofibrate ($P < 0.05$; Fig. 5C).

Collectively, these results demonstrated that fenofibrate attenuated ROS production possibly preventing mitochondrial injury.

Thus, to further explore the mitochondrial protection of fenofibrate and to validate this effect *in vivo*, we analyzed the main mitochondrial proteins involved in the mitochondrial homeostasis.

The protein expression of the key regulator of mitochondrial fusion machinery, mitofusin 2 (Mfn2) and mitochondrial fission, dynamin-related protein 1 (Drp1) in mammals (Marín-García and Akhmedov, 2016) were analyzed. As seen in Fig. 5D, the expression of Mfn2 and Drp1 were dramatically up-regulated in 2K1C-VEH rats when compared with sham-operated rats ($P < 0.01$ for both). Fenofibrate treatment was able to preserve mitochondrial homeostasis (ns versus sham-operated), significantly counteracting the effect of renovascular hypertension on Mfn2 ($P < 0.001$) and Drp1 ($P < 0.01$).

The mitochondrial heathy was also assessed analyzing the biochemical markers of autophagy/mitophagy, as the autophagy initiator beclin-1, Parkin, the microtubule-associated protein1 light chain (LC) 3, as well as the LC3-II/LC3-I ratio, and p62 (Fig. 5D). We found that renovascular hypertension significantly increased the LC3-II/LC3-I ratio ($P < 0.05$), and enhanced the total protein expression of LC3 (LC3-I plus LC3-II) ($P < 0.01$) and beclin-1 ($P < 0.05$). It also decreased the protein expression of Parkin, but it didn't alter the protein expression of p62. Fenofibrate prevented mitochondrial alterations (ns versus sham-operated for all markers). Compared to 2K1C-VEH rats, 2K1C-FFB rats showed a decreased expression of beclin-1 ($P < 0.05$), p62 ($P < 0.01$), total protein expression of LC3 ($P < 0.05$), and similar change of LC3-II/LC3-I ratio ($P = 0.25$). A significant increase of Parkin in 2K1C-FFB rats was also observed ($P < 0.01$).

4. Discussion

The results of the present study demonstrate that fenofibrate effectively counteracts the progression of cardiac hypertrophy and suggest that this protective effect could be exerted partly through a direct effect on mitochondria of cardiomyocytes. Although several data have shown the protective effects of fenofibrate in both *in vivo* and *in vitro* models of cardiac hypertrophy (Jen et al., 2016, 2017; Jia et al., 2014b; Zeng et al., 2018; Zou et al., 2013), to our knowledge, no ones have deeply investigated the mitochondrial protection as possible mechanism. However, interesting data, have reported the relevant role of PPARα-mediated mitochondrial protection in cardiac pathological conditions. Specific cardiac PPARα gene delivery improved cardiac dysfunction by reducing mitochondria-dependent apoptosis and ROS generation in mice with DOX-induced cardiotoxicity (Wang et al., 2020), while nanotized PPARα overexpression improved pathological hypertrophy and cardiac function by ameliorating mitochondrial oxidative stress in 2K1C rats (Rana et al., 2019).

In this work, we found that fenofibrate attenuated cardiac hypertrophic remodeling and reduced the cardiomyocytes size increased by pressure overload. Although fenofibrate slightly lowered blood pressure, our data indicated as these anti-hypertrophic effects could be at least partially pressure independent. Indeed, fenofibrate effectively counteracted the cellular hypertrophy and inhibited the up-regulated mRNA

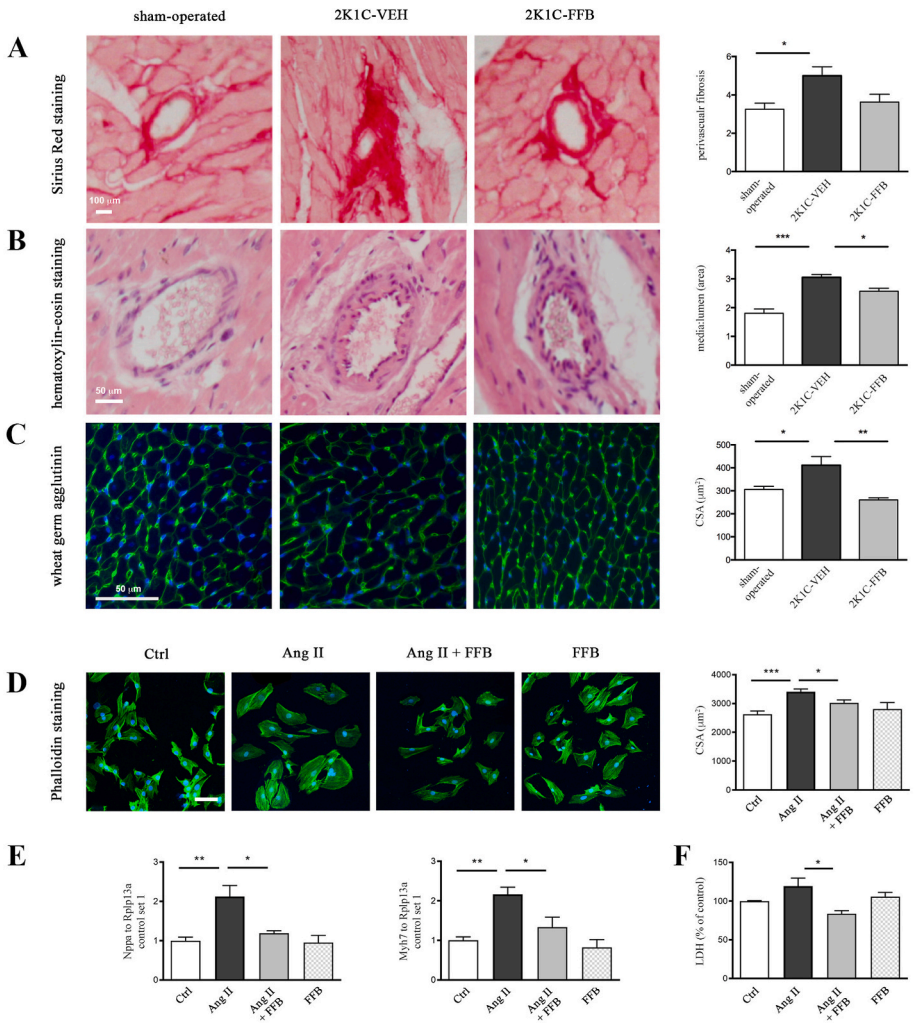

Fig. 3. Fenofibrate reduces cardiac tissue remodeling in 2K1C rats and cellular hypertrophy in Ang II-stimulated H9c2 cells. (A) Representative images of Sirius Red staining of cardiac sections at week 12 (left) and quantification of perivascular fibrosis, measured as ratio of the fibrosis area surrounding the vessel to lumen area (right). Scale bar: 100 μm. **(B)** Representative images of standard hematoxylin-eosin staining of cardiac sections at week 12 (left) and quantification of medial wall thickness of cardiac arteries, measured as vessel media-to-lumen ratio (right). Scale bar: 50 μm. **(C)** Representative images of wheat germ agglutinin staining (green) of cardiac sections at week 12 (left) and quantification of cardiomyocyte cross-sectional area (CSA) (right). Scale bar: 50 μm. **(D)** Representative images of phalloidin staining (green) of H9C2 (left) and quantification of cardiomyocyte cross-sectional area (CSA) (right). Scale bar: 100 μm. **(E)** In H9C2, the mRNA expression levels of hypertrophy marker genes Nppa and Myh7 were normalized by Rplp13a. **(F)** Cytotoxicity (LDH) was measured in cell-free culture supernatants of H9C2.

The bar graphs show the results of the quantitative analysis. Data are shown as means ± SEM, (for *ex vivo*: n = 4/each group; for *in vitro*: n = 3 independent experiments). For *ex vivo*, one-way ANOVA test and post hoc Dunnett's multiple comparisons test (2K1C-VEH group as comparator) were used. For *in vitro*, one-way ANOVA test followed by Sidak multiple comparison "post-hoc" analysis was used. *P < 0.05, **P < 0.01 and ***P < 0.001.

expression of hypertrophic marker genes ANP and β-MHC in Ang II-stimulated H9C2 cells.

Oxidative stress is a common feature of many vascular pathological conditions, such as atherosclerosis, hypertension, and cardiac hypertrophy (Dubois-Deruy et al., 2020), and it is well known that mitochondria are the main organelles associated with ROS production (Murphy, 2009). An elegant study showed that mitochondrial ROS contribute to Ang II-induced myocardial hypertrophy, sustained vascular dysfunction, ROS generation and development of hypertension (Widder et al., 2009). Evidence suggests that fenofibrate may modulate anti-oxidant pathways and improve mitochondrial healthy. Fenofibrate inhibits the ROS production in lipopolysaccharide-treated human umbilical vein endothelial cells (Liu et al., 2011) and in streptozotocin-induced diabetic rats, reducing nephropathy development (Kadian et al., 2013). This anti-oxidant effect is reported to be related with mitochondrial protection in some models of pathological conditions, as paraquat-stimulated retinal/choroidal endothelial cells (Hsu et al., 2020), mice with local heart high dose irradiation (Azimzadeh et al., 2021), radiation-induced skin injury in a rat model and in human keratinocyte HaCaT and skin fibroblast WS1 cells (Sun et al., 2022) and cisplatin-induced ototoxicity in auditory HEI-OC1 cells, organ of Corti with postnatal P3, and adult Balb/c mice (Kim et al., 2018). Here, we found that fenofibrate attenuated the Ang II-induced ROS generation and mitochondrial membrane potential instability. The mitochondrial protection exerted by fenofibrate could be mediated by up-regulation of the Uncoupling protein 2 (UCP2), whose expression is directly modulated by AMPK activation (Hu et al., 2019; Wang et al., 2010). In a previous study on renal damage in salt-loaded SHRSP, we found the role of PPARα in regulating UCP2 expression (Rubattu et al., 2015). UCP2 is a proton transporter that partially dissipates the proton concentration gradient of the inner mitochondria membrane, and plays critical roles in controlling intracellular ROS homeostasis and preventing oxidative stress (Brand and Esteves, 2005). Furthermore, previous studies indicated that UCP2 deficiency exacerbated oxidative stress in

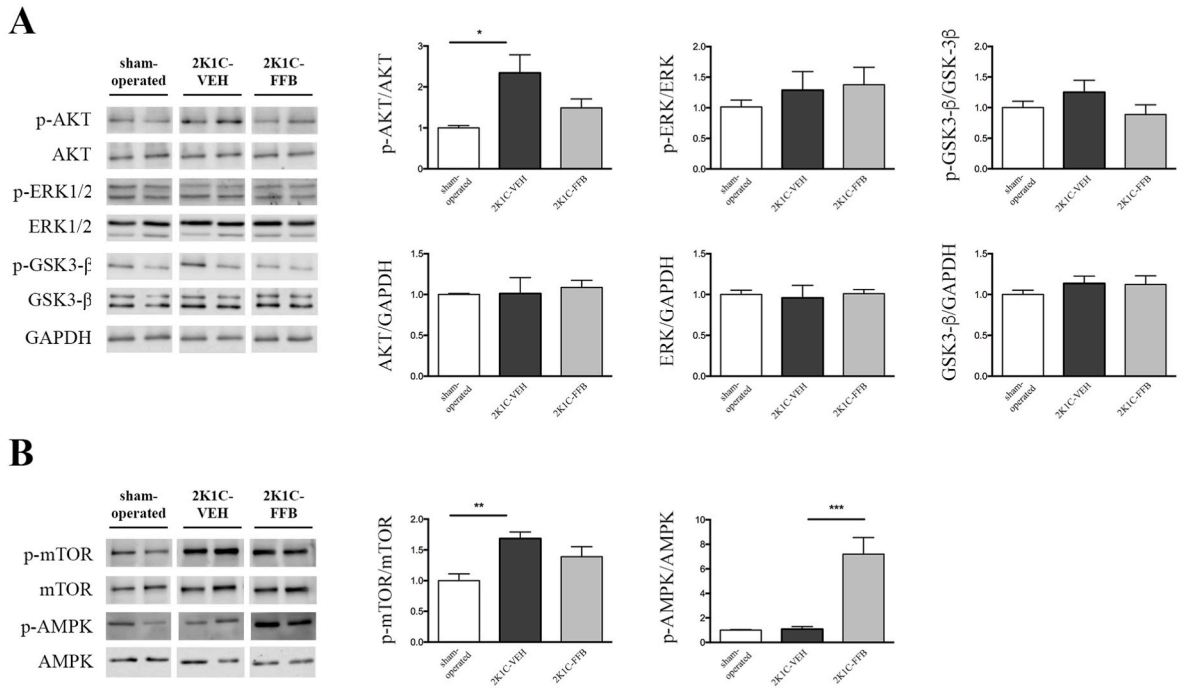

Fig. 4. Fenofibrate attenuates pressure overload-induced activation of ATK/mTOR, and enhances activation of AMPK. (A) Representative immunoblotting analyses of p-AKT, AKT, p-ERK1/2, ERK1/2, p-GSK3-β and GSK3-β, and densitometric analysis of the respective levels, in the hearts at week 12. The expression of p-AKT, p-ERK1/2 and p-GSK3-β was normalized to the level of AKT, ERK1/2, and GSK3-β, respectively, while the expression of AKT, ERK1/2 and GSK3-β was relative to the loading control GAPDH. **(B)** Representative immunoblotting analyses of p-mTOR, mTOR, p-AMPK and AMPK, and densitometric analysis of the respective levels, in the hearts at week 12. The expression of p-mTOR and p-AMPK was normalized to the level of mTOR and AMPK, respectively.
The bar graphs show the results of the quantitative analysis. Data are shown as means ± SEM, (n = 4–6/each group). For statistical analysis one-way ANOVA and post hoc Dunnett's multiple comparisons test (2K1C-VEH group as comparator) or Kruskal-Wallis and post hoc Holm - Bonferroni multiple comparisons test were used. *P < 0.05, **P < 0.01 and ***P < 0.001 vs 2K1C-VEH.

mice (Horimoto et al., 2004), whereas adenovirus-mediated UCP2 overexpression or activation inhibited ROS production and mitochondrial death pathway in neonatal cardiomyocytes (Teshima et al., 2003) and in a mouse model of pulmonary ischemia/reperfusion injury (Chen et al., 2017). Relevantly, the activation of the AMPK/UCP2 signaling pathway improved the indoxyl sulfate-induced hypertrophy in neonatal rat cardiomyocytes (Yang et al., 2015) and the doxorubicin-induced cardiotoxicity in mice and in H9C2 cardiomyoblasts (Hu et al., 2019). Here, we showed a strong decrease of UCP2 protein expression in Ang II-stimulated H9C2 cells and in heart of hypertensive renovascular rats. Thus, besides the well-known anti-oxidant effect, we hypothesize that the UCP2 up-regulation could be, partially, a mechanism through fenofibrate improved the mitochondrial protection and, consequently, cardiac hypertrophy.

We are conscious of some limitation of this study. First, we evaluated the effect of fenofibrate on cardiac hypertrophy, in an experimental condition in which ventricular function was preserved.

No change of ventricular volumes and ejection fraction in severe hypertrophic condition we observed could be explained by the moderate hypertensive condition of 2K1C rats (SBP 146 ± 2 mm Hg, 4 weeks after surgery). Similar results are reported previously in the same model (Mendes et al., 2020), on the contrary, when hypertensive status is severe (SBP ≥180 mm Hg, 4 weeks after surgery) the hypertrophic condition is accompanied by ventricular dysfunction (Chaihongsa et al., 2022).Thus, future studies are need to investigate the effect of fenofibrate on ventricular function in stronger hypertensive models of cardiac hypertrophy.

Second, the anti-hypertrophic effect of fenofibrate could be partially due an overall improvement in global health condition of treated animals, in particular of kidneys. Previous report suggests that fenofibrate improves renal dysfunction and reduced glomerular and tubulointerstitial damage in several models of renal injury (Castiglioni et al., 2018b; Kim et al., 2016). Similarly, in 2K1C rats, fenofibrate could reduce the injury of the clipped and nonclipped kidneys which are responsible of the enhanced plasma renin activity and elevated circulating levels of Ang II (Navar et al., 2002). We are entitled to think that the reduced plasma renin activity, and possibly circulating level of Ang II, contributed in some way to cardiac protection in fenofibrate treated animals. We have already mentioned the possible role of hypertension that has a strong neurogenic component, in particular of the hypothalamic paraventricular nucleus (PVN) and rostral ventrolateral medulla (RVLM) (H.-B. Li et al., 2014). In the 2K1C animal model, oxidative stress and the presence of cytokines within these brain regions play a pivotal role in the hypertensive responses and sympathoexcitation. PPAR-α activation has been reported to decrease neuroinflammation in several brain regions (Chen et al., 2007; Collino et al., 2006), including hypothalamus (Villavicencio-Tejo et al., 2021). Thus, the possible contribution of hypertension in inducing cardiac hypertrophy could be reduced by fenofibrate acting at the level of the central nervous system. Finally, we found a marked alteration in the protein expression of factors regulating autophagy and mitophagy but we didn't investigate at all their activity and mechanism. Therefore, we can't exclude their involvement in the cardioprotective effects of fenofibrate. Growing body of evidence has reported changes in myocardial autophagy in animal models of pressure overload (Li et al., 2016). In particular, autophagosome-lysosome pathway insufficiency, due to reduced lysosomal removal of autophagosomes, was reported in chronic pressure overload-induced cardiac hypertrophy and heart failure (Wang and Cui, 2017). Several studies showed that fenofibrate enhances autophagy although in other research fields than cardiac hypertrophy. Of note, fenofibrate treatment significantly prevented type 1 diabetes-induced cardiac dysfunction and fibrosis improving autophagy (Zhang et al.,

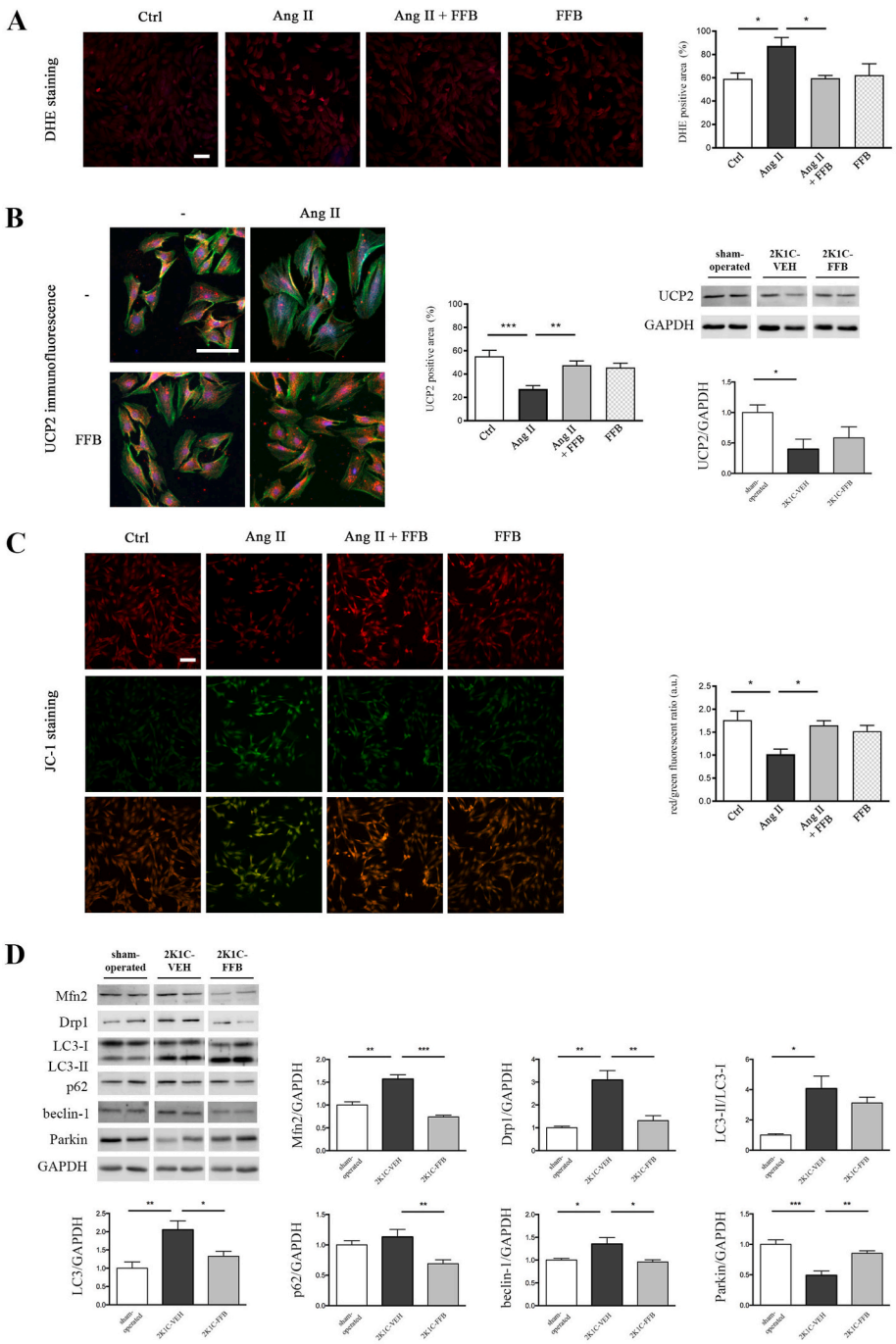

Fig. 5. Fenofibrate attenuates oxidative stress and protects mitochondria.
(A) Representative images of DHE staining of H9C2 (left) and quantification of fluorescent intensity to determine ROS generation (right). Scale bar: 100 μm. **(B)** Effect of fenofibrate on UCP2 in H2C9 and in cardiac tissue. Representative images of UCP2 immunofluorescence of H9C2 and quantification of UCP2 positive area % (left). Scale bar: 50 μm. Representative immunoblotting analyses of UCP2 in the hearts at week 12 (right). **(C)** Representative confocal micrograph showing JC-1staining pattern of H2C9 after different treatment conditions (left). Scale bar: 100 μm. Bar graph shows the quantitative analysis of ratio of red/green fluorescent intensity. **(D)** Representative immunoblotting analyses of Mfn2, Drp1, LC3-I and –II, p62, beclin-1 and Parkin in the hearts at week 12 (left). Quantification of the relative protein levels (right). GAPDH as an internal control.
The bar graphs show the results of the quantitative analysis. Data are shown as means ± SEM, (for *ex vivo*: n = 3–7/each group; for *in vitro*: n = 3 independent experiments). For *ex vivo*, one-way ANOVA test and post hoc Dunnett's multiple comparisons test (2K1C-VEH group as comparator) were used. For *in vitro*, one-way ANOVA test followed by Sidak multiple comparison "post-hoc" analysis was used. *P < 0.05, **P < 0.01 and ***P < 0.001.

2016).

Our *ex-vivo* data suggest that fenofibrate could lead to an improved control of mitochondrial dynamics and enhanced autophagy/mitophagy contributing to the reduction of cardiac hypertrophy and tissue remodeling. Our hypothesis is supported by strong evidence showing that AMP-activated protein kinase (AMPK) activators, as PPARα agonists (Lee and Kim, 2010), inhibit cardiac hypertrophy by promoting autophagy via mTORC1 (Y. Li et al., 2014; Matsumura et al., 2017). Furthermore, in phenylephrine-incubated cardiomyocytes, fenofibrate decreased cell size and mRNA levels of hypertrophic marker genes,

while restored mitochondrial dynamics (Kar and Bandyopadhyay, 2018). In addition to mTORC1, fenofibrate could improve mitochondrial dynamics by UCP2 (Shimasaki et al., 2013). Indeed, UCP2 overexpression activated mitophagy in *in-vivo* and *in-vitro* models of myocardial ischemia/reperfusion (Wu et al., 2019; Geng et al., 2024), acute kidney injury (Qin et al., 2019) and cerebral ischemia (He et al., 2020). A recent study showed that UCP2 silencing reduced autophagy/mitophagy, whereas the opposite was true upon UCP2 overexpression, in endothelial and renal tubular cells (Forte et al., 2021a). UCP2 modulates mitophagy through the regulation of key regulators of mitochondrial dynamics, as PARKIN, mitofusin 2 (Mfn2) and dynamin related protein 1 (Drp1) (Forte et al., 2021a; Geng et al., 2024). All together data suggest that the fenofibrate protective effect we observed on mitochondria could be due to an improved mitochondrial quality control. This one is sustained through synthesis of new mitochondria, fusion and fission (mitochondrial dynamics), and elimination of the damaged mitochondria. The key proteins mediating mitochondrial fusion are Mfn2 (Santel and Fuller, 2001), Drp1 mediates mitochondrial fission (Smirnova et al., 2001). It is well documented that unbalance in the mitochondrial dynamics contribute significantly to cardiac hypertrophy (Forte et al., 2021b).

In this study, we found a significant increase of Mfn2 and Drp1 protein levels in hypertrophic hearts. These results are partially in line with published data. Indeed, the protein expression of Drp1 was shown to increase in hypertrophic hearts of mice with ascending aortic banding (Givvimani et al., 2012) and of high salt-loaded Dahl salt sensitive rats (Hasan et al., 2018). However, the increase of Drp1 doesn't necessary mean an increase of fission preceding mitophagy, since it could represent an increase in the cytosolic fraction which was shown to be up-regulated in the chronic phase of pressure-overloaded when mitophagy is suppressed (Shirakabe et al., 2016). A concurrent increase expression of markers of fusion and fission, including Mfn2 and Drp1, was observed in the heart of subjects with coronary artery disease (Ait-Aissa et al., 2019), suggesting consistent changes in mitochondrial dynamics. On the contrary, Mfn2 expression was down regulated in some models of cardiac hypertrophy and unaltered in hypertrophied hearts with 15 weeks of TAC and in hypertrophied non-infarcted myocardium following MI (Fang et al., 2007). These conflicting results suggest that the expression of Mfn2 could depend on the etiology and time course of hypertrophy. In our model, the increased expression of Mfn2 could be explained by the reduced level of Parkin, an E3 ubiquitin ligase that play a pivotal role in the activation of mitophagy (Dorn, 2016). Indeed, in germline Parkin null mouse hearts, the mRNA levels of the upstream Parkin activator Mfn2 was increased (Bhandari et al., 2014). Besides its role in fusion, Mfn2 appears also to function as a receptor for Parkin and is required for the translocation of Parkin to damaged mitochondria (Chen and Dorn, 2013). Thus, we hypothesize that the increase of Mfn2 could be an adaptive response to overcome the decrease of Parkin or a result of an unbalanced mitochondrial dynamic in which the physiological mitochondrial turnover is altered. Several evidences showed that Parkin depletion, and so reduced mitophagy, induced cardiac hypertrophy and contractile dysfunction in response to pressure-overload (Han et al., 2017) or high-fat diet feeding (Shao et al., 2020; Tong et al., 2019). Here, we found that fenofibrate rebalanced the altered expression of Mfn2, Drp1 and Parkin, suggesting an improved control of mitochondrial dynamics.

The conversion of LC3-I in LC3-II, expressed as LC3-II/LC3-I ratio, is largely use to measure autophagic flux. Here, we observed an increase of LC3-I to LC3-II conversion in hearts of fenofibrate-treated rats, but also in hypertrophic hearts in contrast with previous data (Xie et al., 2018, 2019). We assume that, in our experimental model, LC3-II accumulated in hypertrophic hearts because turnover of LC3-II by autophagic processes was blocked, as previously reported in an *in vitro* assay (Tanida et al., 2005). In line with this aforementioned assumption, we observed an enhanced accumulation of total amount of LC3-I and LC3-II and an unreduced amount of p62 in hypertrophic hearts. Indeed, the level of p62, an indicator of ubiquitinated protein (Pankiv et al., 2007), inversely correlates with autophagic activity (Mizushima et al., 2010), since it is selectively incorporated into autophagosomes through direct binding to LC3 and is efficiently degraded by autophagy (Bjørkøy et al., 2005). The p62 protein expression is commonly increased both in *in-vivo* and *in-vitro* models of cardiac hypertrophy (Liu et al., 2021). Taken together, our data suggest that autophagy is decreased in pressure-overloaded hypertrophic hearts. Instead, fenofibrate promoted the conversion of LC3 I to LC3 II, while decreased the total amount of LC3-I and LC3-II, and of p62, suggesting an enhanced autophagic response. Interestingly, we found that fenofibrate also decreased the protein expression of beclin-1, another protein playing as regulator of autophagy. Indeed, beclin-1 abundance could suppress autophagosome maturation via transcriptional down-regulation of the autophagy-lysosome machinery (Ma et al., 2012). Thus, the increased level of beclin-1 as well as LC3-II means that the autophagic flux was blocked and the autophagic cargo waiting to be degraded as reported in phenylephrine-mediated hypertrophic cardiomyocytes showing a decreased autophagosome removal capacity (Jin et al., 2021). Our data are in line with data obtained with drugs increasing autophagy (Li et al., 2016). The mTORC1 inhibitors, (i.e., rapamycin, sirolimus and everolimus), which are known to improve autophagic flux, have been shown beneficial in various pro-hypertrophic conditions (McMullen et al., 2004; Raichlin et al., 2008; Uchinaka et al., 2017).

5. Conclusion

In conclusion, our study demonstrates for the first time that fenofibrate counteracts cardiac remodeling caused by renovascular hypertension. We have also proved that fenofibrate can sustain mitochondrial function and reduce oxidative stress. We hypothesize that these cardioprotective effects are partially depend on the improvement of the impaired mitochondrial fusion and fission, and on enhanced mitophagy by activation of AMPK/mTORC1 pathway and by enhancing UCP2 expression. Further studies are required to confirm the mechanistic relationship between PPARα, mitophagy and UCP2. Future research are also need to investigate the effectiveness of fenofibrate and the role of PPARα/AMPK/UCP2 axis in other models of cardiac hypertrophy including those not dependent by hypertension. However, we believe that our findings support the repurposing of fenofibrate for the treatment of cardiac hypertrophy and provide new potential targets that mediates its pharmacological function.

Funding

This research did not receive any specific grant from funding agencies in the public, commercial, or not-for-profit sectors.

CRediT authorship contribution statement

Laura Castiglioni: Writing – review & editing, Writing – original draft, Validation, Methodology, Investigation, Formal analysis, Conceptualization. **Paolo Gelosa:** Writing – review & editing, Writing – original draft, Methodology, Formal analysis, Conceptualization. **Majeda Muluhie:** Writing – review & editing, Methodology, Investigation. **Benedetta Mercuriali:** Writing – review & editing, Methodology, Investigation. **Joanna Rzemieniec:** Writing – review & editing, Methodology. **Marco Gotti:** Writing – review & editing, Methodology, Investigation. **Fabio Fiordaliso:** Writing – review & editing, Methodology, Investigation. **Giuseppe Busca:** Writing – review & editing, Investigation. **Luigi Sironi:** Writing – review & editing, Writing – original draft, Validation, Resources, Funding acquisition, Conceptualization.

Declaration of competing interest

The authors declare the following financial interests/personal relationships which may be considered as potential competing interests:

Luigi Sironi reports financial support was provided by University of Milan. Luigi Sironi reports a relationship with University of Milan that includes: employment. If there are other authors, they declare that they have no known competing financial interests or personal relationships that could have appeared to influence the work reported in this paper.

Data availability

Data will be made available on request.

Acknowledgements

The authors thank Dr. Lucia Bena and Dr. Lucia Turolo for excellent technical assistance and Professor Elena Tremoli for fruitful discussion. Part of this work was carried out at NOLIMITS, an advanced imaging facility established by Università degli Studi di Milano.

Appendix A. Supplementary data

Supplementary data to this article can be found online at https://doi.org/10.1016/j.ejphar.2024.176767.

References

Ahmed, S.N., Jhaj, R., Sadasivam, B., Joshi, R., 2020. Regression of the left ventricular hypertrophy in patients with essential hypertension on standard drug therapy. Discoveries 8, e115. https://doi.org/10.15190/d.2020.12.

Ait-Aissa, K., Blaszak, S.C., Beutner, G., Tsaih, S.-W., Morgan, G., Santos, J.H., Flister, M. J., Joyce, D.L., Camara, A.K.S., Gutterman, D.D., Donato, A.J., Porter, G.A., Beyer, A. M., 2019. Mitochondrial oxidative phosphorylation defect in the heart of subjects with coronary artery disease. Sci. Rep. 9, 7623. https://doi.org/10.1038/s41598-019-43761-y.

Akhmedov, A.T., Rybin, V., Marín-García, J., 2015. Mitochondrial oxidative metabolism and uncoupling proteins in the failing heart. Heart Fail. Rev. 20, 227–249. https://doi.org/10.1007/s10741-014-9457-4.

Azimzadeh, O., Subramanian, V., Sievert, W., Merl-Pham, J., Oleksenko, K., Rosemann, M., Multhoff, G., Atkinson, M.J., Tapio, S., 2021. Activation of PPARα by fenofibrate attenuates the effect of local heart high dose irradiation on the mouse cardiac proteome. Biomedicines 9, 1845. https://doi.org/10.3390/biomedicines9121845.

Balakumar, P., Sambathkumar, R., Mahadevan, N., Muhsinah, A. Bin, Alsayari, A., Venkateswaramurthy, N., Dhanaraj, S.A., 2019. Molecular targets of fenofibrate in the cardiovascular-renal axis: a unifying perspective of its pleiotropic benefits. Pharmacol. Res. 144, 132–141. https://doi.org/10.1016/j.phrs.2019.03.025.

Bhandari, P., Song, M., Chen, Y., Burelle, Y., Dorn, G.W., 2014. Mitochondrial contagion induced by Parkin deficiency in Drosophila hearts and its containment by suppressing mitofusin. Circ. Res. 114, 257–265. https://doi.org/10.1161/CIRCRESAHA.114.302734.

Bjørkøy, G., Lamark, T., Brech, A., Outzen, H., Perander, M., Overvatn, A., Stenmark, H., Johansen, T., 2005. p62/SQSTM1 forms protein aggregates degraded by autophagy and has a protective effect on huntingtin-induced cell death. J. Cell Biol. 171, 603–614. https://doi.org/10.1083/jcb.200507002.

Bradford, M., 1976. A rapid and sensitive method for the quantitation of microgram quantities of protein utilizing the principle of protein-dye binding. Anal. Biochem. 72, 248–254. https://doi.org/10.1006/abio.1976.9999.

Brand, M.D., Esteves, T.C., 2005. Physiological functions of the mitochondrial uncoupling proteins UCP2 and UCP3. Cell Metab 2, 85–93. https://doi.org/10.1016/j.cmet.2005.06.002.

Brown, A.J.M., Gandy, S., McCrimmon, R., Houston, J.G., Struthers, A.D., Lang, C.C., 2020. A randomized controlled trial of dapagliflozin on left ventricular hypertrophy in people with type two diabetes: the DAPA-LVH trial. Eur. Heart J. 41, 3421–3432. https://doi.org/10.1093/eurheartj/ehaa419.

Castiglioni, L., Pignieri, A., Fiaschè, M., Giudici, M., Crestani, M., Mitro, N., Abbate, M., Zoja, C., Rottoli, D., Foray, C., Fiordaliso, F., Guerrini, U., Tremoli, E., Sironi, L., Gelosa, P., 2018a. Fenofibrate attenuates cardiac and renal alterations in young salt-loaded spontaneously hypertensive stroke-prone rats through mitochondrial protection. J. Hypertens. 36, 1129–1146. https://doi.org/10.1097/HJH.0000000000001651.

Castiglioni, L., Pignieri, A., Fiaschè, M., Giudici, M., Crestani, M., Mitro, N., Abbate, M., Zoja, C., Rottoli, D., Foray, C., Fiordaliso, F., Guerrini, U., Tremoli, E., Sironi, L., Gelosa, P., 2018b. Fenofibrate attenuates cardiac and renal alterations in young salt-loaded spontaneously hypertensive stroke-prone rats through mitochondrial protection. J. Hypertens. 36, 1129–1146. https://doi.org/10.1097/HJH.0000000000001651.

Chaihongsa, N., Maneesai, P., Sangartit, W., Rattanakanokchai, S., Potue, P., Khamseekaew, J., Bunbupha, S., Pakdeechote, P., 2022. Cardiorenal dysfunction and hypertrophy induced by renal artery occlusion are normalized by galangin treatment in rats. Biomed. Pharmacother. 152, 113231 https://doi.org/10.1016/j.biopha.2022.113231.

Chen, J.-S., Pei, Y., Li, C.-E., Li, Y.-N., Wang, Q.-Y., Yu, J., 2020. Comparative efficacy of different types of antihypertensive drugs in reversing left ventricular hypertrophy as determined with echocardiography in hypertensive patients: a network meta-analysis of randomized controlled trials. J. Clin. Hypertens. 22, 2175–2183. https://doi.org/10.1111/jch.14047.

Chen, K., Xu, Z., Liu, Y., Wang, Z., Li, Y., Xu, X., Chen, C., Xia, T., Liao, Q., Yao, Y., Zeng, Cindy, He, D., Yang, Y., Tan, T., Yi, J., Zhou, J., Zhu, H., Ma, J., Zeng, Chunyu, 2017. Irisin protects mitochondria function during pulmonary ischemia/reperfusion injury. Sci. Transl. Med. 9, eaao6298 https://doi.org/10.1126/scitranslmed.aao6298.

Chen, X.R., Besson, V.C., Palmier, B., Garcia, Y., Plotkine, M., Marchand-Leroux, C., 2007. Neurological recovery-promoting, anti-inflammatory, and anti-oxidative effects afforded by fenofibrate, a PPAR alpha agonist, in traumatic brain injury. J. Neurotrauma 24, 1119–1131. https://doi.org/10.1089/neu.2006.0216.

Chen, Y., Dorn, G.W., 2013. PINK1-Phosphorylated mitofusin 2 is a Parkin receptor for culling damaged mitochondria. Science 340, 471–475. https://doi.org/10.1126/science.1231031, 1979.

Collino, M., Aragno, M., Mastrocola, R., Benetti, E., Gallicchio, M., Dianzani, C., Danni, O., Thiemermann, C., Fantozzi, R., 2006. Oxidative stress and inflammatory response evoked by transient cerebral ischemia/reperfusion: effects of the PPAR-alpha agonist WY14643. Free Radic. Biol. Med. 41, 579–589. https://doi.org/10.1016/j.freeradbiomed.2006.04.030.

Cuspidi, C., Meani, S., Valerio, C., Fusi, V., Sala, C., Maisaidi, M., Zanchetti, A., 2006. Effects of angiotensin II receptor blockade-based therapy with losartan on left ventricular hypertrophy and geometry in previously treated hypertensive patients. Blood Press 15, 107–115. https://doi.org/10.1080/08037050600593052.

da Silva, A.C.A., Severo, J.S., dos Santos, B.L.B., Mendes, P.H.M., Nobre, L.M.S., de Oliveira, A.P., Ferreira, F.C.S., Medeiros, J.V.R., Lima-Junior, R.C., Havt, A., Palheta-Junior, R.C., dos Santos, A.A., Tolentino, M., 2021. Moderate physical exercise activates ATR2 receptors, improving inflammation and oxidative stress in the duodenum of 2K1C hypertensive rats. Front. Physiol. 12 https://doi.org/10.3389/fphys.2021.734038.

Dorn, G.W., 2016. Parkin-dependent mitophagy in the heart. J. Mol. Cell. Cardiol. 95, 42–49. https://doi.org/10.1016/j.yjmcc.2015.11.023.

Dubois-Deruy, E., Peugnet, V., Turkieh, A., Pinet, F., 2020. Oxidative stress in cardiovascular diseases. Antioxidants 9, 864. https://doi.org/10.3390/antiox9090864.

Egan, B.M., 2010. US trends in prevalence, awareness, treatment, and control of hypertension, 1988-2008. JAMA 303, 2043. https://doi.org/10.1001/jama.2010.650.

Fak, A., Okucu, M., Tezcan, H., Bodur, G., Oktay, A., 1996. The effects of amlodipine on left ventricular mass and diastolic function in concentric and eccentric left ventricular hypertrophy. J Cardiovasc Pharmacol Ther 1, 95–100. https://doi.org/10.1177/107424849600100202.

Fang, L., Moore, X.-L., Gao, X.-M., Dart, A.M., Lim, Y.L., Du, X.-J., 2007. Down-regulation of mitofusin-2 expression in cardiac hypertrophy in vitro and in vivo. Life Sci. 80, 2154–2160. https://doi.org/10.1016/j.lfs.2007.04.003.

Forte, M., Bianchi, F., Cotugno, M., Marchitti, S., Stanzione, R., Maglione, V., Sciarretta, S., Valenti, V., Carnevale, R., Versaci, F., Frati, G., Volpe, M., Rubattu, S., 2021a. An interplay between UCP2 and ROS protects cells from high-salt-induced injury through autophagy stimulation. Cell Death Dis. 12, 919. https://doi.org/10.1038/s41419-021-04188-4.

Forte, M., Schirone, L., Ameri, P., Basso, C., Catalucci, D., Modica, J., Chimenti, C., Crotti, L., Frati, G., Rubattu, S., Schiattarella, G.G., Torella, D., Perrino, C., Indolfi, C., Sciarretta, S., 2021b. The role of mitochondrial dynamics in cardiovascular diseases. Br. J. Pharmacol. 178, 2060–2076. https://doi.org/10.1111/bph.15068.

Franzosi, M., Guerrini, U., Castiglioni, L., Sironi, L., Nobili, E., Tremoli, E., Caiani, E.G., 2011. Feasibility of quantitative analysis of regional left ventricular function in the post-infarct mouse by magnetic resonance imaging with retrospective gating. Comput. Biol. Med. 41, 829–837. https://doi.org/10.1016/j.compbiomed.2011.06.021.

Frohlich, E.D., 1999. Risk mechanisms in hypertensive heart disease. Hypertension 34, 782–789. https://doi.org/10.1161/01.HYP.34.4.782.

Gelosa, P., Sevin, G., Pignieri, A., Budelli, S., Castiglioni, L., Blanc-Guillemaud, V., Lerond, L., Tremoli, E., Sironi, L., 2011. Terutroban, a thromboxane/prostaglandin endoperoxide receptor antagonist, prevents hypertensive vascular hypertrophy and fibrosis. Am. J. Physiol. Heart Circ. Physiol. 300, H762–H768. https://doi.org/10.1152/ajpheart.00880.2010.

Geng, Z., Chen, W., Lu, Q., Fu, B., Fu, X., 2024. UCP2 overexpression activates SIRT3 to regulate oxidative stress and mitochondrial dynamics induced by myocardial injury. Arch. Biochem. Biophys. 753, 109918 https://doi.org/10.1016/j.abb.2024.109918.

Givvimani, S., Munjal, C., Tyagi, N., Sen, U., Metreveli, N., Tyagi, S.C., 2012. Mitochondrial division/mitophagy inhibitor (mdivi) ameliorates pressure overload induced heart failure. PLoS One 7, e32388. https://doi.org/10.1371/journal.pone.0032388.

Goldblatt, H., Lynch, J., Hanzal, R.F., Summerville, W.W., 1934. Studies on experimental hypertension. J. Exp. Med. 59, 347–379. https://doi.org/10.1084/jem.59.3.347.

Guazzi, M., Vicenzi, M., Arena, R., Guazzi, M.D., 2011. PDE5 inhibition with sildenafil improves left ventricular diastolic function, cardiac geometry, and clinical status in patients with stable systolic heart failure: results of a 1-year, prospective, randomized, placebo-controlled study. Circ Heart Fail 4, 8–17. https://doi.org/10.1161/CIRCHEARTFAILURE.110.944694.

Gutsol, A.A., Blanco, P., Hale, T.M., Thibodeau, J.F., Holterman, C.E., Nasrallah, R., Correa, J.W.N., Afanasiev, S.A., Touyz, R.M., Kennedy, C.R.J., Burger, D., Hébert, R. L., Burns, K.D., 2022. Comparative analysis of hypertensive nephrosclerosis in animal models of hypertension and its relevance to human pathology. Glomerulopathy. PLoS One 17, 1–22. https://doi.org/10.1371/journal.pone.0264136.

Han, K., Hassanzadeh, S., Singh, K., Menazza, S., Nguyen, T.T., Stevens, M.V., Nguyen, A., San, H., Anderson, S.A., Lin, Y., Zou, J., Murphy, E., Sack, M.N., 2017. Parkin regulation of CHOP modulates susceptibility to cardiac endoplasmic reticulum stress. Sci. Rep. 7, 2093. https://doi.org/10.1038/s41598-017-02339-2.

Hasan, P., Saotome, M., Ikoma, T., Iguchi, K., Kawasaki, H., Iwashita, T., Hayashi, H., Maekawa, Y., 2018. Mitochondrial fission protein, dynamin-related protein 1, contributes to the promotion of hypertensive cardiac hypertrophy and fibrosis in Dahl-salt sensitive rats. J. Mol. Cell. Cardiol. 121, 103–106. https://doi.org/10.1016/j.yjmcc.2018.07.004.

Haslip, M., Dostanic, I., Huang, Y., Zhang, Y., Russell, K.S., Jurczak, M.J., Mannam, P., Giordano, F., Erzurum, S.C., Lee, P.J., 2015. Endothelial uncoupling protein 2 regulates mitophagy and pulmonary hypertension during intermittent hypoxia. Arterioscler. Thromb. Vasc. Biol. 35, 1166–1178. https://doi.org/10.1161/ATVBAHA.114.304865.

He, M., Zhang, T., Fan, Y., Ma, Y., Zhang, J., Jing, L., Li, P.A., 2020. Deletion of mitochondrial uncoupling protein 2 exacerbates mitophagy and cell apoptosis after cerebral ischemia and reperfusion injury in mice. Int. J. Med. Sci. 17, 2869–2878. https://doi.org/10.7150/ijms.49849.

Horimoto, M., Fülöp, P., Derdák, Z., Wands, J.R., Baffy, G., 2004. Uncoupling protein-2 deficiency promotes oxidant stress and delays liver regeneration in mice. Hepatology 39, 386–392. https://doi.org/10.1002/hep.20047.

Hsu, Y.-J., Lin, C.-W., Cho, S.-L., Yang, W.-S., Yang, C.-M., Yang, C.-H., 2020. Protective effect of fenofibrate on oxidative stress-induced apoptosis in retinal–choroidal vascular endothelial cells: implication for diabetic retinopathy treatment. Antioxidants 9, 712. https://doi.org/10.3390/antiox9080712.

Hu, C., Zhang, X., Wei, W., Zhang, N., Wu, H., Ma, Z., Li, L., Deng, W., Tang, Q., 2019. Matrine attenuates oxidative stress and cardiomyocyte apoptosis in doxorubicin-induced cardiotoxicity via maintaining AMPKα/UCP2 pathway. Acta Pharm. Sin. B 9, 690–701. https://doi.org/10.1016/j.apsb.2019.03.003.

Ismael, S., Purushothaman, S., Harikrishnan, V.S., Nair, R.R., 2015. Ligand specific variation in cardiac response to stimulation of peroxisome proliferator-activated receptor-alpha in spontaneously hypertensive rat. Mol. Cell. Biochem. 406, 173–182. https://doi.org/10.1007/s11010-015-2435-x.

Jen, H.-L., Liu, P.-L., Chen, Y.-H., Yin, W.-H., Chen, J.-W., Lin, S.-J., 2016. Peroxisome proliferator-activated receptor α reduces endothelin-1-caused cardiomyocyte hypertrophy by inhibiting nuclear factor- κ B and adiponectin. Mediators Inflamm 1–11. https://doi.org/10.1155/2016/5609121, 2016.

Jen, H.-L., Yin, W.-H., Chen, J.-W., Lin, S.-J., 2017. Endothelin-1-Induced cell hypertrophy in cardiomyocytes is improved by fenofibrate: possible roles of adiponectin. J Atheroscler Thromb 24, 508–517. https://doi.org/10.5551/jat.36368.

Jia, Z., Xue, R., Liu, G., Li, L., Yang, J., Pi, G., Ma, S., Kan, Q., 2014a. HMGB1 is involved in the protective effect of the PPAR α agonist fenofibrate against cardiac hypertrophy. PPAR Res. 2014, 1–9. https://doi.org/10.1155/2014/541394.

Jia, Z., Xue, R., Liu, G., Li, L., Yang, J., Pi, G., Ma, S., Kan, Q., 2014b. HMGB1 is involved in the protective effect of the PPAR α agonist fenofibrate against cardiac hypertrophy. PPAR Res. 2014, 1–9. https://doi.org/10.1155/2014/541394.

Jin, Y.-G., Zhou, H., Fan, D., Che, Y., Wang, Z.-P., Wang, S.-S., Tang, Q.-Z., 2021. TMEM173 protects against pressure overload-induced cardiac hypertrophy by modulating autophagy. J. Cell. Physiol. 236, 5176–5192. https://doi.org/10.1002/jcp.30223.

Kadian, S., Mahadevan, N., Balakumar, P., 2013. Differential effects of low-dose fenofibrate treatment in diabetic rats with early onset nephropathy and established nephropathy. Eur. J. Pharmacol. 698, 388–396. https://doi.org/10.1016/j.ejphar.2012.10.012.

Kar, D., Bandyopadhyay, A., 2018. Targeting peroxisome proliferator activated receptor α (PPAR α) for the prevention of mitochondrial impairment and hypertrophy in cardiomyocytes. Cell. Physiol. Biochem. 49, 245–259. https://doi.org/10.1159/000492875.

Keech, A., Simes, R.J., Barter, P., Best, J., Scott, R., Taskinen, M.R., Forder, P., Pillai, A., Davis, T., Glasziou, P., Drury, P., Kesäniemi, Y.A., Sullivan, D., Hunt, D., Colman, P., D'Emden, M., Whiting, M., Ehnholm, C., Laakso, M., FIELD study investigators, 2005. Effects of long-term fenofibrate therapy on cardiovascular events in 9795 people with type 2 diabetes mellitus (the FIELD study): randomised controlled trial. Lancet 366, 1849–1861. https://doi.org/10.1016/S0140-6736(05)67667-2.

Kim, E.N., Lim, J.H., Kim, M.Y., Kim, H.W., Park, C.W., Chang, Y.S., Choi, B.S., 2016. PPARα agonist, fenofibrate, ameliorates age-related renal injury. Exp. Gerontol. 81, 42–50. https://doi.org/10.1016/j.exger.2016.04.021.

Kim, S.-J., Park, C., Lee, J.N., Park, R., 2018. Protective roles of fenofibrate against cisplatin-induced ototoxicity by the rescue of peroxisomal and mitochondrial dysfunction. Toxicol. Appl. Pharmacol. 353, 43–54. https://doi.org/10.1016/j.taap.2018.06.010.

Kuznetsov, A.V., Javadov, S., Sickinger, S., Frotschnig, S., Grimm, M., Medical, I., Juan, S., 2015. H9c2 and HL-1 cells demonstrates distinct feature of energy metaboolism, mitochondrial function, 1853, 276–284. https://doi.org/10.1016/j.bbamcr.2014.11.015.H9c2.

Lee, W.H., Kim, S.G., 2010. AMPK-dependent metabolic regulation by PPAR agonists. PPAR Res. 1–10. https://doi.org/10.1155/2010/549101, 2010.

Li, H.-B., Qin, D.-N., Ma, L., Miao, Y.-W., Zhang, D.-M., Lu, Y., Song, X.-A., Zhu, G.-Q., Kang, Y.-M., 2014. Chronic infusion of lisinopril into hypothalamic paraventricular nucleus modulates cytokines and attenuates oxidative stress in rostral ventrolateral medulla in hypertension. Toxicol. Appl. Pharmacol. 279, 141–149. https://doi.org/10.1016/j.taap.2014.06.004.

Li, L., Xu, J., He, L., Peng, L., Zhong, Q., Chen, L., Jiang, Z., 2016. The role of autophagy in cardiac hypertrophy. Acta Biochim. Biophys. Sin. 48, 491–500. https://doi.org/10.1093/abbs/gmw025.

Li, Y., Chen, C., Yao, F., Su, Q., Liu, D., Xue, R., Dai, G., Fang, R., Zeng, J., Chen, Y., Huang, H., Ma, Y., Li, W., Zhang, L., Liu, C., Dong, Y., 2014. AMPK inhibits cardiac hypertrophy by promoting autophagy via mTORC1. Arch. Biochem. Biophys. 558, 79–86. https://doi.org/10.1016/j.abb.2014.06.023.

Liu, B.-Y., Li, L., Liu, G.-L., Ding, W., Chang, W.-G., Xu, T., Ji, X.-Y., Zheng, X.-X., Zhang, J., Wang, J.-X., 2021. Baicalein attenuates cardiac hypertrophy in mice via suppressing oxidative stress and activating autophagy in cardiomyocytes. Acta Pharmacol. Sin. 42, 701–714. https://doi.org/10.1038/s41401-020-0496-1.

Liu, J., Lu, C., Li, F., Wang, H., He, L., Hao, Y., Chen, A.F., An, H., Wang, X., Hong, T., Wang, G., 2011. PPAR- α agonist fenofibrate upregulates tetrahydrobiopterin level through increasing the expression of guanosine 5′-triphosphate cyclohydrolase-I in human umbilical vein endothelial cells. PPAR Res. 1–8. https://doi.org/10.1155/2011/523520, 2011.

Ma, X., Liu, H., Foyil, S.R., Godar, R.J., Weinheimer, C.J., Hill, J.A., Diwan, A., 2012. Impaired autophagosome clearance contributes to cardiomyocyte death in ischemia/reperfusion injury. Circulation 125, 3170–3181. https://doi.org/10.1161/CIRCULATIONAHA.111.041814.

Marín-García, J., Akhmedov, A.T., 2016. Mitochondrial dynamics and cell death in heart failure. Heart Fail. Rev. 21, 123–136. https://doi.org/10.1007/s10741-016-9530-2.

Martens, P., Beliën, H., Dupont, M., Vandervoort, P., Mullens, W., 2018. The reverse remodeling response to sacubitril/valsartan therapy in heart failure with reduced ejection fraction. Cardiovasc Ther 36, e12435. https://doi.org/10.1111/1755-5922.12435.

Martin, T.G., Juarros, M.A., Leinwand, L.A., 2023. Regression of cardiac hypertrophy in health and disease: mechanisms and therapeutic potential. Nat. Rev. Cardiol. 20, 347–363. https://doi.org/10.1038/s41569-022-00806-6.

Martinez-Maldonado, M., 1991. Pathophysiology of renovascular hypertension. Hypertension 17, 707–719. https://doi.org/10.1161/01.HYP.17.5.707.

Marx, N., Sukhova, G.K., Collins, T., Libby, P., Plutzky, J., 1999. PPARalpha activators inhibit cytokine-induced vascular cell adhesion molecule-1 expression in human endothelial cells. Circulation 99, 3125–3131. https://doi.org/10.1161/01.cir.99.24.3125.

Matsumura, N., Robertson, I.M., Hamza, S.M., Soltys, C.-L.M., Sung, M.M., Masson, G., Beker, D.L., Dyck, J.R.B., 2017. A novel complex I inhibitor protects against hypertension-induced left ventricular hypertrophy. Am. J. Physiol. Heart Circ. Physiol. 312, H561–H570. https://doi.org/10.1152/ajpheart.00604.2016.

McMullen, J.R., Sherwood, M.C., Tarnavski, O., Zhang, L., Dorfman, A.L., Shioi, T., Izumo, S., 2004. Inhibition of mTOR signaling with rapamycin regresses established cardiac hypertrophy induced by pressure overload. Circulation 109, 3050–3055. https://doi.org/10.1161/01.CIR.0000130641.08705.45.

Mendes, A.S., Blascke de Mello, M.M., Parente, J.M., Omoto, A.C.M., Neto-Neves, E.M., Fazan, R., Tanus-Santos, J.E., Castro, M.M., 2020. Verapamil decreases calpain-1 and matrix metalloproteinase-2 activities and improves hypertension-induced hypertrophic cardiac remodeling in rats. Life Sci. 244, 117153 https://doi.org/10.1016/j.lfs.2019.117153.

Mizushima, N., Yoshimori, T., Levine, B., 2010. Methods in mammalian autophagy research. Cell 140, 313–326. https://doi.org/10.1016/j.cell.2010.01.028.

Murphy, M.P., 2009. How mitochondria produce reactive oxygen species. Biochem. J. 417, 1–13. https://doi.org/10.1042/BJ20081386.

Nah, J., Miyamoto, S., Sadoshima, J., 2017. Mitophagy as a protective mechanism against myocardial stress. In: Comprehensive Physiology. John Wiley & Sons, Inc., Hoboken, NJ, USA, pp. 1407–1424. https://doi.org/10.1002/cphy.c170005.

Navar, L.G., Harrison-Bernard, L.M., Nishiyama, A., Kobori, H., 2002. Regulation of intrarenal angiotensin II in hypertension. Hypertension 39, 316–322. https://doi.org/10.1161/hy0202.103821.

Omura, M., Kobayashi, S., Mizukami, Y., Mogami, K., Todoroki-Ikeda, N., Miyake, T., Matsuzaki, M., 2001. Eicosapentaenoic acid (EPA) induces Ca(2+)-independent activation and translocation of endothelial nitric oxide synthase and endothelium-dependent vasorelaxation. FEBS Lett. 487, 361–366. https://doi.org/10.1016/s0014-5793(00)02351-6.

Pankiv, S., Clausen, T.H., Lamark, T., Brech, A., Bruun, J.-A., Outzen, H., Øvervatn, A., Bjørkøy, G., Johansen, T., 2007. p62/SQSTM1 binds directly to atg8/LC3 to facilitate degradation of ubiquitinated protein aggregates by autophagy. J. Biol. Chem. 282, 24131–24145. https://doi.org/10.1074/jbc.M702824200.

Paoletti, E., Marsano, L., Bellino, D., Cassottana, P., Cannella, G., 2012. Effect of everolimus on left ventricular hypertrophy of de novo kidney transplant recipients: a 1 year, randomized, controlled trial. Transplantation 93, 503–508. https://doi.org/10.1097/TP.0b013e318242be28.

Qin, N., Cai, T., Ke, Q., Yuan, Q., Luo, J., Mao, X., Jiang, L., Cao, H., Wen, P., Zen, K., Zhou, Y., Yang, J., 2019. UCP2-dependent improvement of mitochondrial dynamics protects against acute kidney injury. J. Pathol. 247, 392–405. https://doi.org/10.1002/path.5198.

Raichlin, E., Chandrasekaran, K., Kremers, W.K., Frantz, R.P., Clavell, A.L., Pereira, N.L., Rodeheffer, R.J., Daly, R.C., McGregor, C.G.A., Edwards, B.S., Kushwaha, S.S., 2008.

Sirolimus as primary immunosuppressant reduces left ventricular mass and improves diastolic function of the cardiac allograft. Transplantation 86, 1395–1400. https://doi.org/10.1097/TP.0b013e318189049a.
Rana, S., Datta, R., Chaudhuri, R.D., Chatterjee, E., Chawla-Sarkar, M., Sarkar, S., 2019. Nanotized PPARα overexpression targeted to hypertrophied myocardium improves cardiac function by attenuating the p53-gsk3β-mediated mitochondrial death pathway. Antioxid Redox Signal 30, 713–732. https://doi.org/10.1089/ars.2017.7371.
Roger, V.L., 2013. Epidemiology of heart failure. Circ. Res. 113, 646–659. https://doi.org/10.1161/CIRCRESAHA.113.300268.
Rubattu, S., Di Castro, S., Cotugno, M., Bianchi, F., Mattioli, R., Baima, S., Stanzione, R., Madonna, M., Bozzao, C., Marchitti, S., Gelosa, P., Sironi, L., Pignieri, A., Maldini, M., Giusti, A.M., Nardini, M., Morelli, G., Costantino, P., Volpe, M., 2015. Protective effects of Brassica oleracea sprouts extract toward renal damage in high-salt-fed SHRSP. J. Hypertens. 33, 1465–1479. https://doi.org/10.1097/HJH.0000000000000562.
Rubins, H.B., Robins, S.J., Collins, D., Fye, C.L., Anderson, J.W., Elam, M.B., Faas, F.H., Linares, E., Schaefer, E.J., Schectman, G., Wilt, T.J., Wittes, J., 1999. Gemfibrozil for the secondary prevention of coronary heart disease in men with low levels of high-density lipoprotein cholesterol. Veterans Affairs High-Density Lipoprotein Cholesterol Intervention Trial Study Group. N. Engl. J. Med. 341, 410–418. https://doi.org/10.1056/NEJM199908053410604.
Saberi, S., Cardim, N., Yamani, M., Schulz-Menger, J., Li, W., Florea, V., Sehnert, A.J., Kwong, R.Y., Jerosch-Herold, M., Masri, A., Owens, A., Lakdawala, N.K., Kramer, C. M., Sherrid, M., Seidler, T., Wang, A., Sedaghat-Hamedani, F., Meder, B., Havakuk, O., Jacoby, D., 2021. Mavacamten favorably impacts cardiac structure in obstructive hypertrophic cardiomyopathy: EXPLORER-HCM cardiac magnetic resonance substudy analysis. Circulation 143, 606–608. https://doi.org/10.1161/CIRCULATIONAHA.120.052359.
Santel, A., Fuller, M.T., 2001. Control of mitochondrial morphology by a human mitofusin. J. Cell Sci. 114, 867–874.
Schirone, L., Forte, M., Palmerio, S., Yee, D., Nocella, C., Angelini, F., Pagano, F., Schiavon, S., Bordin, A., Carrizzo, A., Vecchione, C., Valenti, V., Chimenti, I., De Falco, E., Sciarretta, S., Frati, G., 2017. A review of the molecular mechanisms underlying the development and progression of cardiac remodeling. Oxid. Med. Cell. Longev. 1–16. https://doi.org/10.1155/2017/3920195, 2017.
Sciarretta, S., Volpe, M., Sadoshima, J., 2014. Mammalian target of rapamycin signaling in cardiac physiology and disease. Circ. Res. 114, 549–564. https://doi.org/10.1161/CIRCRESAHA.114.302022.
Sealey, J.E., Gordon, R.D., Mantero, F., 2005. Plasma renin and aldosterone measurements in low renin hypertensive states. Trends in Endocrinology & Metabolism 16, 86–91. https://doi.org/10.1016/j.tem.2005.02.006.
Shao, D., Kolwicz, S.C., Wang, P., Roe, N.D., Villet, O., Nishi, K., Hsu, Y.-W.A., Flint, G.V., Caudal, A., Wang, W., Regnier, M., Tian, R., 2020. Increasing fatty acid oxidation prevents high-fat diet-induced cardiomyopathy through regulating parkin-mediated mitophagy. Circulation 142, 983–997. https://doi.org/10.1161/CIRCULATIONAHA.119.043319.
Shimasaki, Y., Pan, N., Messina, L.M., Li, C., Chen, K., Liu, L., Cooper, M.P., Vita, J.A., Keaney, J.F., 2013. Uncoupling protein 2 impacts endothelial phenotype via p53-mediated control of mitochondrial dynamics. Circ. Res. 113, 891–901. https://doi.org/10.1161/CIRCRESAHA.113.301319.
Shirakabe, A., Zhai, P., Ikeda, Y., Saito, T., Maejima, Y., Hsu, C.-P., Nomura, M., Egashira, K., Levine, B., Sadoshima, J., 2016. Drp1-Dependent mitochondrial autophagy plays a protective role against pressure overload–induced mitochondrial dysfunction and heart failure. Circulation 133, 1249–1263. https://doi.org/10.1161/CIRCULATIONAHA.115.020502.
Smirnova, E., Griparic, L., Shurland, D.-L., van der Bliek, A.M., 2001. Dynamin-related protein Drp1 is required for mitochondrial division in mammalian cells. Mol. Biol. Cell 12, 2245–2256. https://doi.org/10.1091/mbc.12.8.2245.
Smith, S.H., Bishop, S.P., 1986. Selection criteria for drug-treated animals in two-kidney, one clip renal hypertension. Hypertension 8, 700–705. https://doi.org/10.1161/01.HYP.8.8.700.
Sporková, A., Čertíková Chábová, V., Doleželová, Š., Jíchová, Š., Kopkan, L., Vaňourková, Z., Kompanowska-Jezierska, E., Sadowski, J., Maxová, H., Červenka, L., 2017. Fenofibrate attenuates hypertension in Goldblatt hypertensive rats: role of 20-hydroxyeicosatetraenoic acid in the nonclipped kidney. Am. J. Med. Sci. 353, 568–579. https://doi.org/10.1016/j.amjms.2017.04.009.
Sun, C., Song, B., Sheng, W., Yu, D., Yang, T., Geng, F., Fang, K., Jiao, Y., Zhang, J., Zhang, S., 2022. Fenofibrate attenuates radiation-induced oxidative damage to the skin through fatty acid binding protein 4 (FABP4). Frontiers in Bioscience-Landmark 27, 214. https://doi.org/10.31083/j.fbl2707214.
Sun, S., Lu, F., Zhao, Y., Liu, Z., Wang, S., 2011. Effects and reversal of left ventricular hypertrophy of amlodipine plus amiloride/hydrochlorothiazide versus amlodipine plus telmisartan in patients with mild to moderate hypertension. Int. J. Cardiol. 152, S24. https://doi.org/10.1016/j.ijcard.2011.08.543.
Tanida, I., Minematsu-Ikeguchi, N., Ueno, T., Kominami, E., 2005. Lysosomal turnover, but not a cellular level, of endogenous LC3 is a marker for autophagy. Autophagy 1, 84–91. https://doi.org/10.4161/auto.1.2.1697.
Teshima, Y., Akao, M., Jones, S.P., Marbán, E., 2003. Uncoupling protein-2 overexpression inhibits mitochondrial death pathway in cardiomyocytes. Circ. Res. 93, 192–200. https://doi.org/10.1161/01.RES.0000085581.60197.4D.
Thöne-Reineke, C., Olivier, J., Godes, M., Zart, R., George, I., Bauer, C., Neumayer, H.-H., Hocher, B., 2003. Effects of angiotensin-converting enzyme inhibition and calcium channel blockade on cardiac apoptosis in rats with 2K1C (two-kidney/one-clip) renovascular hypertension. Clin. Sci. (Lond.) 104, 79–85, 10.1042/.
Tian, X.Y., Ma, S., Tse, G., Wong, W.T., Huang, Y., 2018. Uncoupling protein 2 in cardiovascular health and disease. Front. Physiol. 9 https://doi.org/10.3389/fphys.2018.01060.
Tong, M., Saito, T., Zhai, P., Oka, S., Mizushima, W., Nakamura, M., Ikeda, S., Shirakabe, A., Sadoshima, J., 2019. Mitophagy is essential for maintaining cardiac function during high fat diet-induced diabetic cardiomyopathy. Circ. Res. 124, 1360–1371. https://doi.org/10.1161/CIRCRESAHA.118.314607.
Torrealba, N., Aranguiz, P., Alonso, C., Rothermel, B.A., Lavandero, Rs, 2017. Mitochondria in structural and functional cardiac remodeling. In: Mitochondrial Dynamics in Cardiovascular Medicine, pp. 277–306. https://doi.org/10.1007/978-3-319-55330-6_15.
Uchinaka, A., Yoneda, M., Yamada, Y., Murohara, T., Nagata, K., 2017. Effects of mTOR inhibition on cardiac and adipose tissue pathology and glucose metabolism in rats with metabolic syndrome. Pharmacol Res Perspect 5, e00331. https://doi.org/10.1002/prp2.331.
Vásquez-Trincado, C., García-Carvajal, I., Pennanen, C., Parra, V., Hill, J.A., Rothermel, B.A., Lavandero, S., 2016. Mitochondrial dynamics, mitophagy and cardiovascular disease. J. Physiol. 594, 509–525. https://doi.org/10.1113/JP271301.
Villavicencio-Tejo, F., Flores-Bastías, O., Marambio-Ruiz, L., Pérez-Reytor, D., Karahanian, E., 2021. Fenofibrate (a PPAR-α agonist) administered during ethanol withdrawal reverts ethanol-induced astrogliosis and restores the levels of glutamate transporter in ethanol-administered adolescent rats. Front. Pharmacol. 12, 653175 https://doi.org/10.3389/fphar.2021.653175.
Wagner, K.-D., Wagner, N., 2020. PPARs and myocardial infarction. Int. J. Mol. Sci. 21 https://doi.org/10.3390/ijms21249436.
Wang, W., Fang, Q., Zhang, Z., Wang, D., Wu, L., Wang, Y., 2020. PPARα ameliorates doxorubicin-induced cardiotoxicity by reducing mitochondria-dependent apoptosis via regulating MEOX1. Front. Pharmacol. 11 https://doi.org/10.3389/fphar.2020.528267.
Wang, X., Cui, T., 2017. Autophagy modulation: a potential therapeutic approach in cardiac hypertrophy. Am. J. Physiol. Heart Circ. Physiol. 313, H304–H319. https://doi.org/10.1152/ajpheart.00145.2017.
Wang, Y., Nishi, M., Doi, A., Shono, T., Furukawa, Y., Shimada, T., Furuta, H., Sasaki, H., Nanjo, K., 2010. Ghrelin inhibits insulin secretion through the AMPK-UCP2 pathway in β cells. FEBS Lett. 584, 1503–1508. https://doi.org/10.1016/j.febslet.2010.02.069.
Widder, J.D., Fraccarollo, D., Galuppo, P., Hansen, J.M., Jones, D.P., Ertl, G., Bauersachs, J., 2009. Attenuation of angiotensin II–induced vascular dysfunction and hypertension by overexpression of thioredoxin 2. Hypertension 54, 338–344. https://doi.org/10.1161/HYPERTENSIONAHA.108.127928.
Wu, H., Ye, M., Liu, D., Yang, Jian, Ding, J., Zhang, J., Wang, X., Dong, W., Fan, Z., Yang, Jun, 2019. UCP2 protect the heart from myocardial ischemia/reperfusion injury via induction of mitochondrial autophagy. J. Cell. Biochem. 120, 15455–15466. https://doi.org/10.1002/jcb.28812.
Xie, X., Bi, H.-L., Lai, S., Zhang, Y.-L., Li, N., Cao, H.-J., Han, L., Wang, H.-X., Li, H.-H., 2019. The immunoproteasome catalytic β5i subunit regulates cardiac hypertrophy by targeting the autophagy protein ATG5 for degradation. Sci. Adv. 5, eaau0495. https://doi.org/10.1126/sciadv.aau0495.
Xie, Y.-P., Lai, S., Lin, Q.-Y., Xie, X., Liao, J.-W., Wang, H.-X., Tian, C., Li, H.-H., 2018. CDC20 regulates cardiac hypertrophy via targeting LC3-dependent autophagy. Theranostics 8, 5995–6007. https://doi.org/10.7150/thno.27706.
Yang, K., Xu, X., Nie, L., Xiao, T., Guan, X., He, T., Yu, Y., Liu, L., Huang, Y., Zhang, J., Zhao, J., 2015. Indoxyl sulfate induces oxidative stress and hypertrophy in cardiomyocytes by inhibiting the AMPK/UCP2 signaling pathway. Toxicol. Lett. 234, 110–119. https://doi.org/10.1016/j.toxlet.2015.01.021.
Zeng, S.-Y., Lu, H.-Q., Yan, Q.-J., Zou, J., 2018. A reduction in ADAM17 expression is involved in the protective effect of the PPAR- α activator fenofibrate on pressure overload-induced cardiac hypertrophy. PPAR Res. 1–8. https://doi.org/10.1155/2018/7916953, 2018.
Zhang, J., Cheng, Y., Gu, J., Wang, S., Zhou, S., Wang, Y., Tan, Y., Feng, W., Fu, Y., Mellen, N., Cheng, R., Ma, J., Zhang, C., Li, Z., Cai, L., 2016. Fenofibrate increases cardiac autophagy via FGF21/SIRT1 and prevents fibrosis and inflammation in the hearts of Type 1 diabetic mice. Clin Sci 130, 625–641. https://doi.org/10.1042/CS20150623.
Zhou, Y., He, X., Chen, Y., Huang, Y., Wu, L., He, J., 2015. Exendin-4 attenuates cardiac hypertrophy via AMPK/mTOR signaling pathway activation. Biochem. Biophys. Res. Commun. 468, 394–399. https://doi.org/10.1016/j.bbrc.2015.09.179.
Zhu, G.-Q., Xu, Y., Zhou, L.-M., Li, Y.-H., Fan, L.-M., Wang, W., Gao, X.-Y., Chen, Q., 2009. Enhanced cardiac sympathetic afferent reflex involved in sympathetic overactivity in renovascular hypertensive rats. Exp. Physiol. 94, 785–794. https://doi.org/10.1113/expphysiol.2008.046565.
Zhu, Z.-Y., Gao, T., Huang, Y., Xue, J., Xie, M.-L., 2016. Apigenin ameliorates hypertension-induced cardiac hypertrophy and down-regulates cardiac hypoxia inducible factor-1α in rats. Food Funct. 7, 1992–1998. https://doi.org/10.1039/C5FO01464F.
Zou, J., Le, K., Xu, S., Chen, J., Liu, Z., Chao, X., Geng, B., Luo, J., Zeng, S., Ye, J., Liu, P., 2013. Fenofibrate ameliorates cardiac hypertrophy by activation of peroxisome proliferator-activated receptor-α partly via preventing p65-NFκB binding to NFATc4. Mol. Cell. Endocrinol. 370, 103–112. https://doi.org/10.1016/j.mce.2013.03.006.